UNIVERSITY OF EMBU

DAVID MUSYOKA KINYILI

MSc

2019

CRAMÉR-RAO BOUND OF DIRECTION FINDING USING UNIFORM CIRCULAR ARRAY AND 2-CIRCLE CONCENTRIC UNIFORM ARRAY

DAVID MUSYOKA KINYILI (MSc)

A RESEARCH PROJECT SUBMITTED IN PARTIAL FULFILLMENT FOR AWARD OF THE DEGREE OF MASTER OF SCIENCE IN APPLIED MATHEMATICS OF THE UNIVERSITY OF EMBU

SEPTEMBER, 2019

DECLARATION

This project report is my original work and has not been presented for a degree in any other university.

Signature..... Date.....

Musyoka Kinyili
B527/1145/2017
Department of Mathematics, Computing, and Information Technology.

This project report has been submitted for examination with our approval as university supervisors.

Signature..... Date.....

Dr. Dominic Makaa Kitavi, PhD.
Department of Mathematics, Computing, and Information Technology,
University of Embu.

Signature..... Date.....

Dr. Cyrus Gitonga Ngari, PhD.
Department of Mathematics, Computing, and Information Technology,
University of Embu.

DEDICATION

I sincerely wish to dedicate my research work to my loving family members including my beloved father, mother, brothers and sisters who supported me endlessly and unfailing. May the heavenly father bless and grant you un-shaking health and long life. I additionally dedicate the work to my beloved friends Moses John and Esther Mbithe for their moral and spiritual support throughout my research work duration and thereafter. May you always remain supportive especially in times of need and keep up your good work.

ACKNOWLEDGMENT

The knowledge extension and innovative research project on direction-of-arrival estimation problem using the proposed sensor-array grid based on Cramér-Rao bound has been quite rewarding and interesting. Many researchers ventured on this field of direction finding before me and through their works, they have been actually prolific contributers to my success in this project by acting as strong pillars and stepping grounds for accomplishment of my research. I wish to particularly thank Prof. Kainam Thomas Wong who has done lots of work on both electromagnetic and acoustic sensors in direction finding using different algorithms. He gave me the first glimpse to develop this project and has continuously supported me through provision of extensive and brilliant ideas to accomplish this project.
My sincere gratitude goes to my two supervisors, Dr. Dominic Makaa Kitavi and Dr. Cyrus Gitonga Ngari for they have been an ideal team who tirelessly and whole-heartedly helped me throughout the project. I thank Dr. Kitavi for his confidence in me, his help to me to learn and be a pro in LATEX and MAT-LAB softwares and always motivating me to accomplish a significant task at specified time. I also thank Dr. Ngari for his encouragement to work ahead of the time limit, finish my tasks earlier and importantly helping me to maneuver a way to draw neat and standard diagrams.
To the staff and technicians in the department of Mathematics, Computing and Information Technology who helped me whenever I called for assistance, thank you and please continue with your good work.
I sincerely thank the University of Embu Board of Postgraduate Studies, for awarding me the scholarship to further my studies for through that, you made an important step to keep my dreams alive. Thank you all.

TABLE OF CONTENTS

LIST OF FIGURES

LIST OF APPENDICES

LIST OF ABBREVIATIONS

AoA	Angle-of-Arrival
ARV	Array Response Vector
CRB	Cramér-Rao Bound
CRB(θ)	Cramér-Rao Bound of θ
CRB(ϕ)	Cramér-Rao Bound of ϕ
CRLB	Cramér-Rao Lower Bound
CUCA	Concentric Uniform Circular Array
DF	Direction Finding
DoA	Direction-of-Arrival
ESPRIT	Estimation of Signal Parameters via Rotational Invariance Technique
$\exp$	Exponential
FIM	Fisher Information Matrix
MLE	Maximum Likelihood Estimator
MSE	Mean Square Error
MUSIC	MUltiple SIgnal Classification
MVU	Minimum Variance Unbiased
1-D	One Dimension
PDF	Probability Distribution Function
3-D	Three Dimensions
2-D	Two Dimensions
UCA	Uniform Circular Array
ULA	Uniform Linear Array
URA	Uniform Rectangular Array
Var	Variance

LIST OF SYMBOLS

$\in$	Element of
ϕ	phi for azimuth angle
θ	theta for polar angle
$[\cdot]^T$	Transposition of the term inside the square brackets
c	Propagation speed
λ	lambda for wavelength
ω	omega for $2\pi f$
$\mathbf{a}(\theta)$	Array manifold with respect to θ
σ_n^2	Noise variance
σ_s^2	Signal variance
$\mathbf{I}_{LM}$	Identity matrix of size $LM \times LM$
$\forall$	for all
f	Frequency
φ	Varphi for signal phase
μ	mu for mean
$E[\cdot]$	Expectation of the term inside the square brackets
$\otimes$	otimes for Kronecker product
$\mathbf{\Gamma}$	Gamma for covariance matrix
ξ	xi for collection of parameters to be estimated
$*$	asterisk for off diagonal elements not of interest in the investigation
$[\cdot]^{-1}$	Inverse of the term inside the square brackets
$\mathrm{Re}\{\cdot\}$	Real-valued part of the entity inside the curly brackets
$\mathrm{Tr}\{\cdot\}$	Trace of the entity inside the curly brackets
$[\cdot]^H$	Conjugate transposition of the term in the square brackets

ABSTRACT

Source direction-of-arrival estimation problem has received much attention in recent years following its significant role in array-signal processing and wide range of applications such as radar, wireless communication, sonar, seismology among others. Direction finding has been solved by several techniques such as Maximum likelihood estimator, MUltiple Signal Classification, Estimation of Parameters via Rotational Invariance Technique and Cramér-Rao bound using array of sensors in both uniformly-spaced and non-uniformly-spaced. The sensors have further been arranged in different geometric patterns ranging from one-dimension to three-dimensional. However, little effort has been made in direction finding using concentric planar arrays with fixed centers at the Cartesian origin. In this study, a new planar sensor-array geometry (the 2-circle concentric uniform array geometry) centered at the Cartesian origin, that maximizes the array's spatial aperture mainly for bivariate azimuth-polar resolution of direction-of-arrival estimation problem was proposed. The proposed geometry provides almost invariant azimuth angle coverage and offers the advantage of full rotational symmetry (circular invariance) while maintaining an inter-sensor spacing not exceeding half wavelength (for non-ambiguity with respect to the Cartesian direction cosines) among other advantages. The study adopted Cramér-Rao bound technique of direction finding via a uniform circular array (single ring array) and the proposed geometry to estimate the bivariate azimuth-polar angles-of-arrival. Both the array manifolds and the Cramér-Rao bounds for the uniform circular array and that of the proposed array grid were derived. Further, a better-accurate performance in direction finding of the proposed array grid over that of the single ring array grid was analytically verified under different constraints of investigation. It was found that the proposed sensor-array geometry has better estimation accuracy than a single ring array and the 2-circle concentric uniform array geometry would have the best estimation accuracy for minimal number of sensors hence reducing the hardware cost. The study therefore recommends that the 2-circle concentric uniform array geometry should be used for direction finding with minimal number of sensors and with an inter-sensor spacing not exceeding half a wavelength as opposed to a uniform circular array geometry.

CHAPTER ONE

INTRODUCTION

1.1 Background Information

Problem of estimating angle-of-arrival (AoA) of a plane wave (or multiple plane waves) is commonly referred to as direction finding (DF) or direction-of-arrival (DoA) estimation problem [5]. It finds its application in radar, medical diagnosis and treatment, electronic surveillance, radio astronomy [40], position location and tracing systems [63]. This is because it is a major method of location determination, in security services especially by reconnaissance of radio communications of criminal organization and in military intelligence by detecting activities of potential enemies and gaining information on enemy's communication order [12]. Due to its diverse application and difficulty of obtaining the optimum estimator, the topic has attracted a significant amount of attention over the last several decades.

Several techniques exist to address the problem of estimating azimuth-polar AoA of multiple sources using the signal received at the array of sensors [21]. Some of the already used methods of DF are: Maximum likelihood estimator (MLE) [6], MUSIC (MUltiple SIgnal Classification) which is a highly popular eigenstructure-based direction-of-arrival estimation problem method applicable to a non-uniformly spaced array of sensors [3], ESPRIT (Estimation of Signal Parameters via Rotational Invariance Technique) [4], Cramér-Rao Bound (CRB) which has been found to be the most accurate technique in DF and the simplest due to its simplicity in computations [10], and other techniques. The knowledge of a reference signal or direction of the desired signal source is required in the application of array processing to achieve its desired objectives.

Antenna array are widely used to solve direction finding problem. For instance, in radar application, the antenna array are useful for air-traffic control and target acquisition. They have been used by intelligence agencies for covert location of transmission and signal interception. For example, in airport surveillance to determine the range, an electromagnetic pulse that is reflected by the aircraft is transmitted, causing the echo to be received by

the antenna after seconds [63]. In wireless communication, DoA estimation may significantly improve efficiency in communication and network capacity, support and enhance location-aided routing, dynamic network and different types of location-related services and applications [57].

In sonar, in which the interest is the position of a target, such as submarine, the target radiates noise due to machinery on board, propeller action, etc. This noise which is actually the signal of interest propagates through and is received by array of sensors. The sensors' output are then transmitted to tow ship for input to a digital computer. Because of the sensors' positions, relative to the arrival angle of the target signal, the signal is received in speech processing systems. A particularly important problem is speech recognition which is the recognition of speech by a machine (digital computers) [1]. For example in recognizing individual speech sounds or phonemes (i.e vowels, consonants etc).

Furthermore, the direction-of-arrival (DoA) estimation problem has been widely discussed in both uniformly-spaced and non-uniformly-spaced isotropic sensors. The aim of DF is to estimate azimuth(ϕ)-polar(θ) angles of arrival [38], which are respectively measured counterclockwise from the positive x-axis and clockwise from the positive z-axis with, $\phi \in [0, 2\pi)$ and $\theta \in \left[0, \frac{\pi}{2}\right]$ [77]. The sensors are arranged in different geometric patterns mainly to improve the estimation performance in which the geometric patterns include: Uniform linear array (ULA), uniform circular array (UCA), uniform rectangular array (URA) [5], regular tetrahedral array, collocated triad of orthogonal dipoles [77], and L-shaped 2-dimensional array [7], [66]. Notably, signal impinging/arriving on sensors is usually affected by noise (undesired random disturbances) which lower accuracy and precision of estimation of the signal's parameters. The noise could be caused by undetected variations in temperature, pressure, humidity etc. Noise can also occur as a result of imprecision of sensors' components [57].

Of all the array geometries, circular and concentric circular arrays alone provides almost invariant azimuth angle coverage and offers full rotational symmetry about the origin, thereby realizing azimuthal invariance (with the azimuth defined on the circular plane) as well as increasing array's spatial aperture [24, 17, 13, 27, 39, 62, 9, 18] . Furthermore, a sensor-array's spatial resolution in the azimuth and elevation, increases with the size of the array's aperture. As evidenced in [42, 41, 43, 2], recent research has focused on strategies to enlarge this aperture without additional sensors. However, one difficult on widening array's aperture is to avoid side and grating lobes in beam-forming and and also to avoid cyclic

ambiguities in direction finding [32, 20, 9, 8, 11]; these problems would be encountered if the inter-sensor spacing exceeds half a wavelength, thereby violating the spatial version of the Nyquist sampling theorem. This now raises two alarming questions that, **could a two-ring array geometry have better-accurate estimation performance in direction finding than a single ring array geometry? If true then, how may the circular array aperture be widened without additional (isotropic) sensors while maintaining the inter-sensor spacing not to exceed half-wavelength?** Answering these questions will display effectiveness and accuracy of using the two-circle concentric uniform array geometry over the single ring array geometry in direction finding via the Cramér-Rao bound. Thus, the study proposed a new planar sensor-array grid termed as 2-circle concentric uniform array geometry or concentric uniform circular array (CUCA) geometry centered at the Cartesian origin, that maintains an inter-sensor spacing of $\leq$ half a wavelength (to avoid ambiguity in the estimated direction-of-arrival), that provides almost invariant azimuth angle coverage and retains the advantage of full rotational symmetry, and that maximizes the array's spatial aperture, with only little/no increase in the number of sensors. The inter-sensor spacing here was equal to $2R_{\mathrm{UCA}} \sin\left(\frac{\pi}{L_{\mathrm{UCA}}}\right)$, where L_{UCA} and R_{UCA} denotes the number of isotropic sensors on the circumference of a circle and the radius respectively. As a result, the study presented derivation of the array manifolds and the Cramér-Rao bounds for both the proposed array grid and that of the single ring array and finally compared the performance of the proposed array grid to that of a single ring array grid in direction finding.

1.2 Statement of the Problem

The concept of direction finding (DF) has been extensively discussed on both uniformly-spaced and non-uniformly-spaced isotropic sensors. These sensors have been arranged in different geometric patterns which are either one-dimensional (1-D), two-dimensional (2-D) or three-dimensional (3-D). Some of the already discussed and existing array of sensors include: orthogonal L-shaped array of sensors, regular tetrahedral array of sensors, uniform linear array (ULA) of sensors, uniform rectangular array (URA) of sensors and uniform circular array (UCA) of sensors. Array manifold vectors for the above mentioned array of sensors have been derived together with their corresponding Cramér-Rao bounds under the underlying dimensions (1-D, 2-D or 3-D). Furthermore, as evidenced in [64], [77], [10], [6], [5], [3], studies have drawn much attention on direction finding using different methods such as MLE, MUSIC, and ESPRIT in comparison to the Cramér-Rao bound (CRB) technique under different geometric patterns of sensors. Their general conclusion has been that, the Cramér-Rao bound method is the most accurate for it provides a lower bound on the accuracy of any unbiased estimator. However, very scanty literature is available on DF using concentric planar array of sensors with fixed centers at the Cartesian origin. For instance, little effort has been made in introducing these arrays, but whose centers are not fixed and are not necessarily centered at the Cartesian origin. Due to this therefore, a new planar sensor-array grid termed as the two-circle concentric uniform array or the concentric uniform circular array (CUCA) geometry offering the aforementioned advantages was proposed . Hence with reference to the already existing array manifolds and Cramér-Rao bounds for both uniformly-spaced and non-uniformly-spaced geometric array of sensors, derivation of both the array manifolds and the Cramér-Rao bounds for uniform circular array and the proposed geometry both lying on the x-y plane (planar) and centered at the Cartesian origin were presented and further, fundamental analysis of the Cramér-Rao bounds for the proposed array grid under different constraints of investigation and comparison of their performance was carried out. The results of the study would provide a deeper understanding as well as extension of knowledge for the concept of direction finding using concentric arrays to their somewhat counter-intuitive terms of concentric planar arrays with fixed centers at the Cartesian origin.

1.3 Justification of the Study

As aforementioned, little effort has been made in introducing concentric planar array of sensors whose centers are not fixed and are not necessarily centered at the Cartesian origin, as evidenced by the scanty literature available about these planar arrays with fixed centers at the Cartesian origin. Thus, a need cropped up to conduct a study. In this study, a new sensor-array geometry was proposed. Results of the study would equip and benefit direction finders such as seismologists, security officers, electronic surveyors, medical diagnosis doctors among others, to improve on direction finding.

1.4 Objectives of the Study

1.4.1 Main Objective

The broad objective of the study was to compare the performance of uniform circular array and a two-circle concentric uniform array geometries in direction finding.

1.4.2 Specific Objectives

The specific objectives of the study were:

(i) To find array manifolds for a uniform circular array and a two-circle concentric uniform array geometry,

(ii) To derive Cramér-Rao bound for azimuth-polar angles-of-arrival using uniform circular array and a two-circle concentric uniform array, and

(iii) To give fundamental analysis of Cramér-Rao bound for the two-circle concentric uniform array geometry under different constraints of investigation.

1.5 Significance of the Study

The study results aims at giving an insightful understanding of the concept of direction finding (DF) using planar concentric arrays as well as setting an avenue for further research in a new but closely related area of two-circle concentric uniform array.

CHAPTER TWO

LITERATURE REVIEW

2.1 Introduction

This chapter presents a review of related literature on the concept of direction finding (DF). This is done in several sections which discuss review on circular arrays of sensors, the advantages of circular arrays over the other geometric patterns, the concept of array manifold, mathematical data model, unbiased and biased estimators, minimum variance criterion and the Cramér-Rao bound as a technique of direction-of-arrival (DoA) estimation problem which was used in this project. Moreover, some existing results for the above mentioned sections are also presented.

2.2 Review on a Uniform Circular Array (UCA) of Sensors

The uniform (single-ring) circular array has been investigated for direction finding using different algorithms such as MLE, MUSIC, ESPRIT, CRB in [5, 46, 48, 49, 50, 17, 53, 54, 24, 59, 29, 32, 68] . The corresponding Cramer-Rao bound has been derived in closed-form in [1, 10, 64, 69], but only in an open form in [44, 56, 61, 64, 67, 70], and only plotted (but not derived) in comparison to the other algorithms in [3, 45, 47, 50, 57, 58, 74, 78]. Here, the overall conclusion has been that, the Cramer-Rao bound is the most accurate algorithm giving the most accurate estimates in direction finding.

2.3 Advantages of Circular Arrays Over the Other Geometric Patterns

As evidenced in [9, 13, 18, 39, 29], the circular arrays are the most advantageous geometric patterns used in direction finding over the other aforementioned geometric pattern. Some of these advantages include: They provide almost invariant azimuth angle coverage, they are flexible in array pattern and design, they offer full rotational symmetry and they can yield invariant array pattern over a certain frequency band for beam-forming in 3-dimensions. Notably, since concentric arrays are still circular, they also enjoy the above mentioned merits.

2.4 The Concept of Array Manifold

Array manifold vector also known as the steering vector is the set of array responses of a signal or the data received on the array from incoming signal for all azimuth-polar angles. The array manifold is the locus of all array response vector (manifold vector) and maps the geometrical aspects of the array system to the signal environment. Findings in [51] have indicated that the array manifold vector plays a key role of modeling the response of an array of omni-directional elements in the case of unity powered signal impinging on the array from direction (θ, ϕ), with respect to the array reference point and the chosen system of coordinates. It should be noted that an assumption of the plane wave propagation is made for the derivation of manifold vector.

In order to estimate any parameter of a signal, knowledge of array manifold is key. Depending on the pattern of the sensor-array used, array manifold vector varies. The array manifold vector can be in 1-dimensional (1-D), 2-dimensional (2-D) or 3-dimensional (3-D) depending on the geometric pattern of the sensors.

From [10], the following examples of array manifolds for linear and circular arrays, are given respectively. For simplicity, we suppose that the antennas and the emitters are on the same plane so that the array manifold can be characterized by polar angle only.

Linear Array: Consider a linear array with M omni-directional antenna elements separated by distance of d_m, from a common reference point in the array. Suppose θ is the direction measured from the line perpendicular to the array. Then, the array manifold is

given by

$$\mathbf{a}(\theta) = \begin{bmatrix} \exp\left\{j\frac{2\pi d_1}{\lambda}\sin(\theta)\right\} \\ \exp\left\{j\frac{2\pi d_2}{\lambda}\sin(\theta)\right\} \\ \vdots \\ \exp\left\{j\frac{2\pi d_M}{\lambda}\sin(\theta)\right\} \end{bmatrix}.$$

Where λ is the signal's wavelength and $j = \sqrt{-1}$.

Circular Array: Consider a circular array with radius R and M antenna elements. For omni-directional elements, the array manifold is given by

$$\mathbf{a}(\theta) = \begin{bmatrix} \exp\left\{j\frac{2\pi R}{\lambda}\sin(\theta-\theta_1)\right\} \\ \exp\left\{j\frac{2\pi R}{\lambda}\sin(\theta-\theta_2)\right\} \\ \vdots \\ \exp\left\{j\frac{2\pi R}{\lambda}\sin(\theta-\theta_M)\right\} \end{bmatrix},$$

where θ_i (for $i = 1, 2, \cdots M$) are the element angles relative to the center of the circle.

2.5 Mathematical Data Model

The observed data vector for any particular geometric pattern would be given by $\mathbf{z} = \mathbf{a}s(m) + \mathbf{n}(m)$ for $m = 1, 2, 3, \cdots, M$ where $\mathbf{a}$ is the array manifold vector, $s(m)$ is the incident signal, $\mathbf{n}(m)$ is additive noise and m is the time instant.

Signal arriving on a sensor array are usually affected by noise which lower the accuracy and precision of estimation of signal's parameters. The noise in most receiving systems consists of internal and external noise [57]. The external noise is defined as an unwanted random disturbances that is intercepted by the sensors while internal noise is produced by the electronic devices and includes thermal noise and weak versions of other signals in the system such as clocks and oscillators. If the system is designed well, such that the antennas are free of mutual coupling, and it is assumed that the thermal noise is dormant, a good model for the noise is white Gaussian noise with covariance matrix of $\sigma_n^2\mathbf{I}$, where σ_n^2 is the noise power, and $\mathbf{I}$ is an identity matrix.

Results in [64], [77] have shown that, suppose an array of L number of isotropic sensors is separately located in space. Denote the ℓ^{th} sensors' three-dimensional location as

(x_ℓ, y_ℓ, z_ℓ). Consider an incident signal of wave-length λ, impinging upon the array from a polar angle of $\theta \in \left[0, \frac{\pi}{2}\right]$, measured from the positive z-axis in the clockwise direction and an azimuth angle of $\phi \in [0, 2\pi)$, measured from the positive x-axis in the counterclockwise direction. To this incident signal, the array response may be defined by an $L \times 1$ array manifold whose ℓ^{th} entry equals

$$[\mathbf{a}]_\ell \;=\; g_\ell \exp\left\{ j\frac{2\pi}{\lambda}\left[x_\ell \sin(\theta)\cos(\theta) + y_\ell \sin(\theta)\sin(\theta) + z_\ell \cos(\theta)\right]\right\}$$

$\forall\, \ell = 1, 2, \cdots, L$.

The L sensors together would produce the below $L \times 1$ snapshots at any discrete-time instant m:

$$\mathbf{x}(m) \;=\; \sigma_s \mathbf{a} s(m) + \mathbf{n}(m)$$

where $\{s(m)\ \forall\ m\}$ represents the incident signal and $\{\mathbf{n}(m)\ \forall\ m\}$ denotes the additive noise. The incident signal is pure-tone complex-valued defined by, $s(m) = \sigma_s \exp\{j(2\pi f m + \varphi)\}$ where the frequency of f and the phase of φ are prior known, whereas the amplitude of σ_s is unknown but deterministic. The additive noise $[\mathbf{n}(m)]_\ell$ is circularly complex-valued Gaussian, with a mean of zero and a variance of σ_n^2, spatio-temporally white over both ℓ and m, hence a spatial correlation of $\mathbf{\Gamma}_n = \sigma_n^2 \mathbf{I}_L$.

Based on M number of snapshots $\{\mathbf{x}(m), m = 1, 2, \cdots, M\}$, the aim of direction-finding problem is to estimate (θ, ϕ), which are modeled as deterministic constants. The data's distribution is normal/Gaussian with a mean of

$$\mu = E[\mathbf{x}] = \mathbf{s} \otimes \mathbf{a}$$

and a covariance matrix of

$$\mathbf{\Gamma} \;=\; \sigma_n^2 \mathbf{I}_{(LM \times LM)}.$$

Here, $\otimes$ denotes the Kronecker product, and $E[\cdot]$ represents statistical expectation of the entity inside the square brackets.

Furthermore, if a narrow-band source could be emitting a signal $s(t)$ of wavelength λ in the direction of array of M co-planar sensors, then the far-field source could be seen at antenna array under DF angle of θ restricted to $[-\pi, \pi]$ with respect to the x-axis measured in the

clockwise direction. The array output at time instant t could be given by

$$\mathbf{z}(t) \quad = \quad \mathbf{a}(\theta)s(t) + \mathbf{n}(t),$$

where $t = t_1, t_2 \cdots, t_N$, is a scaled and noise-corrupted replica of the DoA-dependent Array Response Vector (ARV) $\mathbf{a}(\theta)$ [34]. The ARV is an extension of the array steering vector that incorporates gain of the sensors. The purpose of the snapshots $(\mathbf{z}(t)), t = t_1, t_2 \cdots, t_N$ is to estimate the parameter θ using a variety of techniques. The following statistical properties are often assumed about $s(t)$ and $\mathbf{n}(t)$: $s(t)$ and $\mathbf{n}(t)$ are independent, $\mathbf{n}(t)$ is a zero-mean Gaussian distributed with a covariance $E[\mathbf{n}(t)\mathbf{n}^H(t)] = \sigma_n^2\mathbf{I}$, for $\mathbf{I}$ being $M \times M$ identity matrix and $s(t)$ are assumed to be either deterministic unknown parameter or independent zero-mean circular Gaussian distributed with variance of σ_s^2.

2.6 Unbiased Estimators

Estimators are functions of sample observations used to estimate any unknown parameter of interest [52]. The expectations are that, a good estimator should result in an estimate value that is close to the true value of the parameter being estimated. An estimator is said to be unbiased if on average, the estimator yields the true value of the unknown parameter [1]. Since the parameter to be estimated may lie anywhere in the open interval $a < \phi < b$, unbiased estimator ascertains that no matter what the true value of ϕ is, the estimator will definitely yield it on the average. Thus, unbiasedness serves as a measure of closeness between an estimator and the parameter. For instance, an estimator $\tilde{\phi}$ is an unbiased estimator of ϕ if the mean or expectation of $\tilde{\phi}$ over all possible samples is ϕ. Mathematically, an estimator is unbiased if $E(\tilde{\phi}) = \phi$, $\phi \in (a, b)$ where (a, b) denotes the range of possible values of ϕ. On the other hand, biased estimators are ones that are characterized by systematic errors, which presumably should not be present.

2.7 Minimum Variance Criterion

In order to obtain optimal estimators, we need to adopt some optimality criterion as evidenced in [1]. A natural one is the mean square error (MSE), defined as

$$MSE(\tilde{\phi}) \quad = \quad E\left[(\tilde{\phi} - \phi)^2\right].$$

This measures the average mean square deviation of any estimator from the true value. However, it's unfortunate that adoption of this natural criterion may lead to unrealizable estimators, which cannot be written solely as a function of data. To understand the problem which results, let's rewrite the MSE as

$$\begin{aligned} MSE(\tilde{\phi}) &= E\left\{\left[(\tilde{\phi}-E(\tilde{\phi}))^2+(E(\tilde{\phi}-\phi))\right]^2\right\} \\ &= Var(\tilde{\phi})+\left[E(\tilde{\phi})-\phi\right]^2 \\ &= Var(\tilde{\phi})+b^2(\phi). \end{aligned}$$

This implies that the MSE is composed of errors due to the variance of the estimator as well as the bias [55], [1]. It would seem that any criterion which depends on the bias will lead to unrealizable estimator. Although this generally holds, on occasion, realizable minimum MSE estimator can be found by alternatively constraining the bias to zero and finding the estimator which minimizes the variance. Such estimator is termed as the minimum variance unbiased (MVU) estimator. The MVU commonly used is the Cramér-Rao lower bound (CRLB) or just the Cramér-Rao bound (CRB). It should be noted that, the MSE is just the variance [52].

2.8 The Cramér-Rao Bound (CRB)

The Cramér-Rao bound is a useful tool for assessing the accuracy of parameter estimation method as it provides a lower bound on the accuracy of any unbiased estimator. Thus, for any unbiased estimator $\tilde{\phi}$ as indicated in [10], we have

$$MSE(\tilde{\phi}) = Var(\tilde{\phi}) \geq CRB.$$

The CRB provides an algorithm-independent benchmark against which various algorithms can be compared.

In addition, the Cramér-Rao bound provides a lower bound to the estimation variance of an unbiased estimator [77]. To find the CRB for estimating the azimuth-polar angles-of-arrival, the inverse of Fisher information matrix (FIM) is computed. The Fisher information matrix represents the way to measure the information about the parameter contained in the observations or the amount of information that an observable random variable carries about an unknown parameter [60], [22]. Moreover, the Fisher information matrix determines how

much information a measurement brings about the parameters that index the underlying probability distribution for the measurement [63].

For a complex Gaussian data model vector, the $(i,j)^{th}$ entry of the FIM is be given by

$$[\mathbf{F}(\boldsymbol{\xi})]_{i,j} = 2\mathrm{Re}\left\{\left[\frac{\partial \boldsymbol{\mu}}{\partial \boldsymbol{\xi}_i}\right]^H \boldsymbol{\Gamma}^{-1}\frac{\partial \boldsymbol{\mu}}{\partial \boldsymbol{\xi}_j}\right\} + \mathrm{Tr}\left\{\boldsymbol{\Gamma}^{-1}\frac{\partial \boldsymbol{\Gamma}}{\partial \boldsymbol{\xi}_\mathrm{i}}\boldsymbol{\Gamma}^{-1}\frac{\partial \boldsymbol{\Gamma}}{\partial \boldsymbol{\xi}_\mathrm{j}}\right\} \tag{2.1}$$

[15] where $\mathrm{Re}\{\cdot\}$ symbolizes the real-value part of the entity inside the curly brackets, $\mathrm{Tr}\{\cdot\}$ signifies the trace of the contents inside the curly brackets and the superscript ^{H} denotes the conjugate transposition [64], [5]. For instance, if we collect the two parameters to be estimated as entries in a 2×1 vector $\boldsymbol{\xi} := [\theta, \phi]$, the FIM will have a $(k,r)^{th}$ entry of (2.1) and thus the FIM will be give by

$$\mathbf{F}(\boldsymbol{\xi}) = \begin{bmatrix} F_{\theta,\theta} & F_{\theta,\phi} \\ F_{\phi,\theta} & F_{\phi,\phi} \end{bmatrix}, \tag{2.2}$$

where

$$F_{\theta,\theta} = 2\mathrm{Re}\left\{\left[\frac{\partial \boldsymbol{\mu}}{\partial \theta}\right]^H \boldsymbol{\Gamma}^{-1}\frac{\partial \boldsymbol{\mu}}{\partial \theta}\right\} + \mathrm{Tr}\left\{\boldsymbol{\Gamma}^{-1}\frac{\partial \boldsymbol{\Gamma}}{\partial \theta}\boldsymbol{\Gamma}^{-1}\frac{\partial \boldsymbol{\Gamma}}{\partial \theta}\right\},$$

$$F_{\theta,\phi} = 2\mathrm{Re}\left\{\left[\frac{\partial \boldsymbol{\mu}}{\partial \theta}\right]^H \boldsymbol{\Gamma}^{-1}\frac{\partial \boldsymbol{\mu}}{\partial \phi}\right\} + \mathrm{Tr}\left\{\boldsymbol{\Gamma}^{-1}\frac{\partial \boldsymbol{\Gamma}}{\partial \theta}\boldsymbol{\Gamma}^{-1}\frac{\partial \boldsymbol{\Gamma}}{\partial \phi}\right\},$$

$$F_{\phi,\theta} = 2\mathrm{Re}\left\{\left[\frac{\partial \boldsymbol{\mu}}{\partial \phi}\right]^H \boldsymbol{\Gamma}^{-1}\frac{\partial \boldsymbol{\mu}}{\partial \theta}\right\} + \mathrm{Tr}\left\{\boldsymbol{\Gamma}^{-1}\frac{\partial \boldsymbol{\Gamma}}{\partial \phi}\boldsymbol{\Gamma}^{-1}\frac{\partial \boldsymbol{\Gamma}}{\partial \theta}\right\},$$

and

$$F_{\phi,\phi} = 2\mathrm{Re}\left\{\left[\frac{\partial \boldsymbol{\mu}}{\partial \phi}\right]^H \boldsymbol{\Gamma}^{-1}\frac{\partial \boldsymbol{\mu}}{\partial \phi}\right\} + \mathrm{Tr}\left\{\boldsymbol{\Gamma}^{-1}\frac{\partial \boldsymbol{\Gamma}}{\partial \phi}\boldsymbol{\Gamma}^{-1}\frac{\partial \boldsymbol{\Gamma}}{\partial \phi}\right\},$$

where $\boldsymbol{\mu}$ and $\boldsymbol{\Gamma}$ are the mean and the covariance matrix of the observed data model respectively [38], [77].

The inverse of (2.2) gives the 2×2 Cramér-Rao bound matrix

$$\begin{bmatrix} \mathrm{CRB}(\theta) & * \\ * & \mathrm{CRB}(\phi) \end{bmatrix} = \begin{bmatrix} F_{\theta,\theta} & F_{\theta,\phi} \\ F_{\phi,\theta} & F_{\phi,\phi} \end{bmatrix}^{-1},$$

where $*$ refers to entries not of interest to the present research. Using the above approach,

$$\mathrm{CRB}(\theta) = \frac{F_{\phi,\phi}}{F_{\theta,\theta}F_{\phi,\phi} - F_{\theta,\phi}F_{\phi,\theta}}$$

and

$$\mathrm{CRB}(\phi) = \frac{F_{\theta,\theta}}{F_{\theta,\theta}F_{\phi,\phi} - F_{\theta,\phi}F_{\phi,\theta}}.$$

CHAPTER THREE

RESEARCH METHODOLOGY

3.1 Introduction

In order to complete the project successfully, solid background knowledge of DF was very useful. Particularly, the Cramér-Rao bound algorithm of direction-of-arrival estimation problem was used to estimate the unknown but deterministic bivariate azimuth-polar angles-of-arrival.

3.1.1 Study Geometries

The Uniform circular array geometry (UCA)

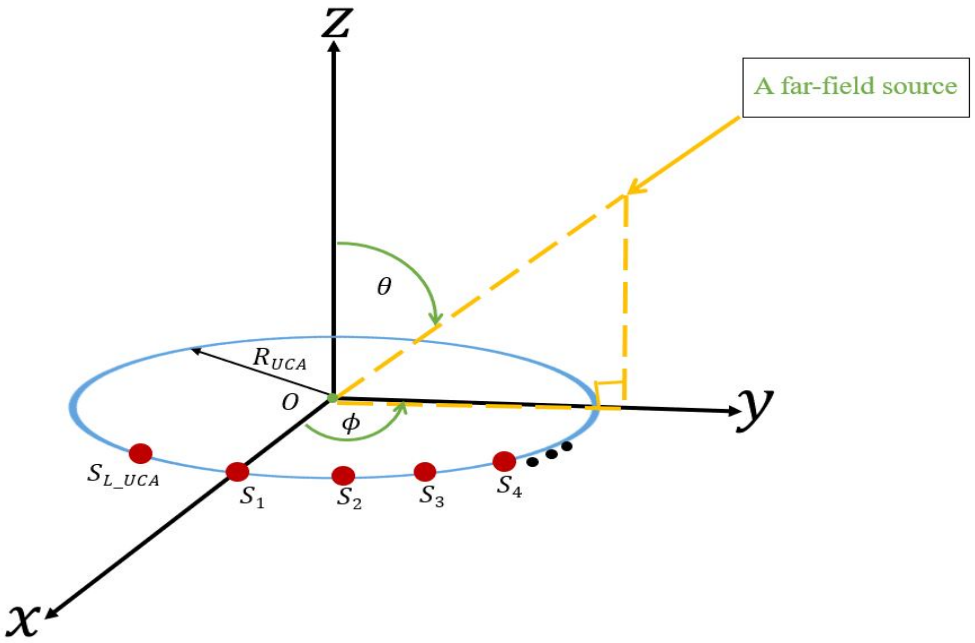

Figure 3.1: A single ring array geometry with equal spaced isotropic sensors.

The 2-circle concentric uniform array geometry

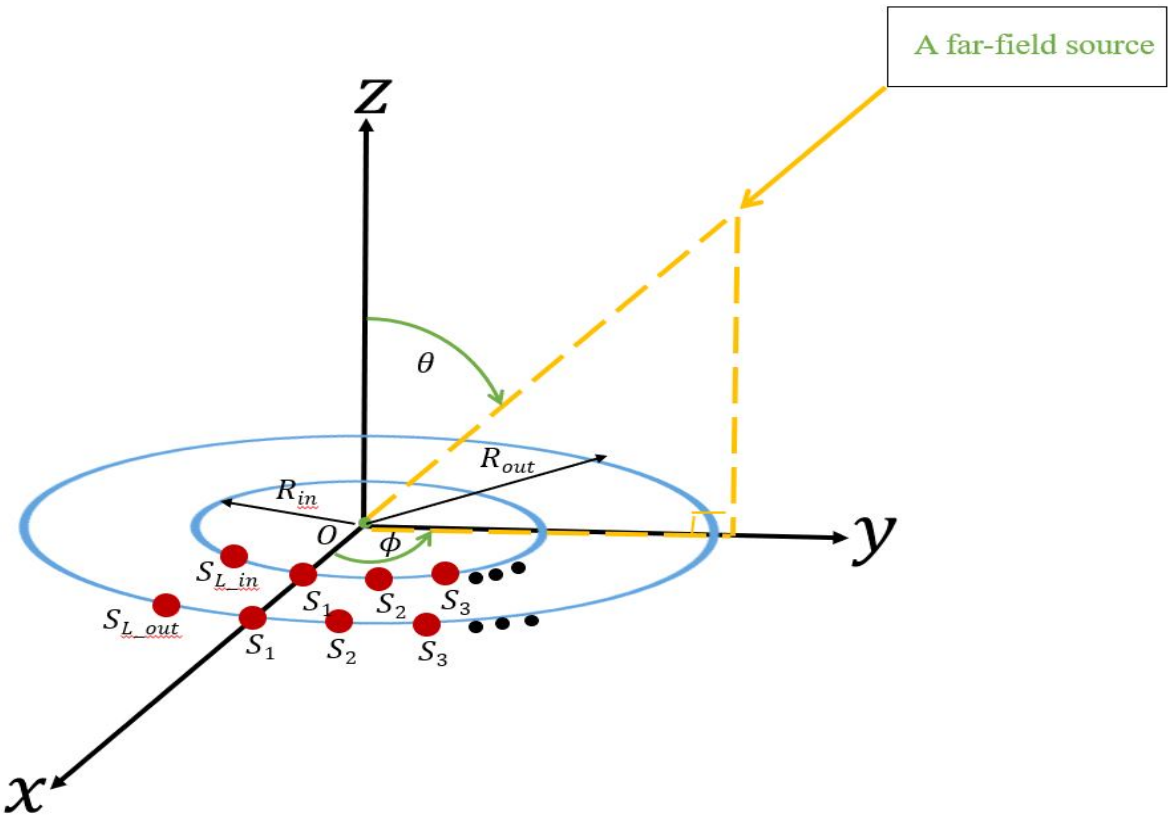

Figure 3.2: A two-ring array geometry of equidistant isotropic sensors.

The UCA and the CUCA were both centered at the Cartesian origin denoted by O and thus the origin was considered as the reference point. Moreover, finite number of isotropic sensors arranged on the circumference of the circles with uniform inter-sensor spacing (not exceeding half a wavelength) were used.

3.1.2 Softwares

The LATEX and the MAT-LAB softwares were used for typing the report (because of the tricky-complicated equation encountered) and plotting comparative graphs respectively.

3.2 Objective 1: Array Manifold Vector Derivation

To derive the array manifolds for the UCA and the CUCA geometries, the following steps were used systematically:

1. The Cartesian coordinates showing the general location of the sensors with respect to x, y and z-axes were determined,

2. Equation representing the set of observations received by the array of sensors with respect to time, t, and the position vector, $\mathbf{p}$ was found. Notably, this observations equation was in terms of time domain signal,

3. The time domain signal obtained in (2) above was converted into frequency domain signal by taking the Fourier transform of the observations equation, and

4. Finally, the targeted array manifold vector was deduced from the newly formed frequency domain equation in (3) above by simply adopting the complex part.

3.3 Objective 2: Derivation of the Cramér-Rao Bound

To derive the Cramér-Rao bound for both the uniform circular array and the concentric 2-circle array geometries, the below steps were systematically followed:

1. The array manifolds derived in objective (1) above were adopted,

2. The data model which shows the equation representation of the observed data vector for any particular geometric pattern of sensors was formulated,

3. The Fisher Information matrix (FIM) which measures the amount of information that a certain random variable carries about an unknown parameter was computed,

4. The inverse of the (FIM) was computed to obtain a Cramér-Rao bound matrix, and

5. Lastly, the required $\mathrm{CRB}(\theta)$ and the $\mathrm{CRB}(\phi)$ were deduced from the Cramér-Rao bound matrix obtained in (4) above.

NOTE:*The derivations for each step above are extensively discussed in chapter 4 for the results.*

3.4 Objective 3: The Fundamental Analysis

To give the fundamental analysis of the CRBs, different constraints of investigation (closed equations showing the relationship between the number of sensors for both the UCA and the CUCA geometries and also the relationship between the radii of the CUCA geometry) were proposed and used. Further, comparison in performance in direction finding for the UCA and the CUCA geometries was done by plotting comparative graphs of their CRBs against the number of sensors and the radii using the MAT-LAB software.

CHAPTER FOUR

RESULTS

4.1 Array Manifold Vector Derivation

In this section, the array manifold vector for the uniform circular array geometry is first derived and further used to derive the array manifold vector for the proposed array geometry.

4.1.1 The Uniform Circular Array (UCA)

Consider a circle centered at the Cartesian origin and of radius R_{UCA}. Suppose L_{UCA} number of isotropic sensors are uniformly spaced on the circle's circumference, as illustrated in figure 4.1. The origin denoted by O was considered as the reference point. Further,

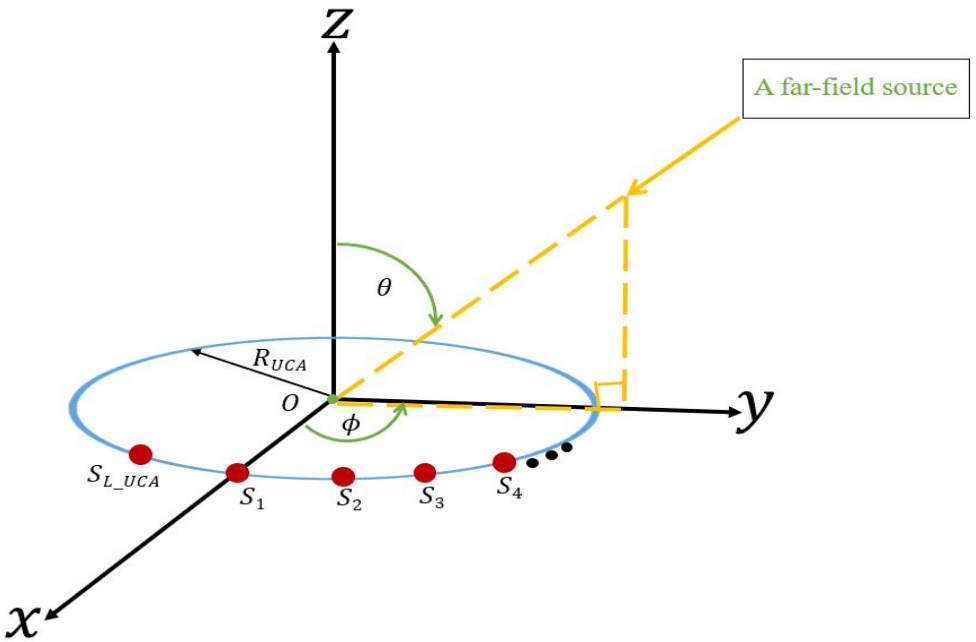

Figure 4.1: A uniform circular array of isotropic sensors.

considering the arrival of wave(s), say a plane wave(s) for example, then the wave(s) impinge on O at an azimuth angle of ϕ and a polar angle of θ measured counterclockwise,

and clockwise, from the positive x-axis and positive z-axis, respectively.

$S_1, S_2, S_3, \cdots, S_{L_{\mathrm{UCA}}}$ were let to be points denoting location of an array consisting of a set of the isotropic sensors. Furthermore, the sensors were unidirectionally arranged in which the direction could be either counterclockwise or just clockwise from the positive x-axis. The circumference of the circle was given by $2\pi R_{\mathrm{UCA}}$, and since there were L_{UCA} number of sensors, then it followed easily that the inter-sensor spacing (spacing between any two consecutive sensors) was $\frac{2\pi R_{\mathrm{UCA}}}{L_{\mathrm{UCA}}}$. Generally, the location of the ℓ^{th} sensor in terms of Cartesian coordinates was denoted by $\mathbf{p}_\ell$ and defined as

$$\mathbf{p}_\ell \;=\; \left[R_{\mathrm{UCA}}\cos\left(\frac{2\pi(\ell-1)}{L_{\mathrm{UCA}}}\right),\; R_{\mathrm{UCA}}\sin\left(\frac{2\pi(\ell-1)}{L_{\mathrm{UCA}}}\right),\; 0\right]^T,$$

for $\ell = 1, 2, 3, \cdots, L_{\mathrm{UCA}}$, where $x = R\cos\left(\frac{2\pi(\ell-1)}{L_{\mathrm{UCA}}}\right)$, $y = R\sin\left(\frac{2\pi(\ell-1)}{L_{\mathrm{UCA}}}\right)$ and $z = 0$ where ^{T} denotes transposition. With the information stated above, the main aim was to derive array manifold vector for the UCA denoted by $\mathbf{a}_{\mathrm{UCA}}(\theta, \phi)$, as follows:

4.1.2 Observations at the Array of Sensors

Let $\mathbf{y}(t)$ to be the signal that would be received on point O at time instant t, such that the observations at the array of sensors with respect to time instances t and position vector $\mathbf{p}$ would be given by,

$$\mathbf{y}(t, \mathbf{p}) \;=\; \begin{bmatrix} y(t-\tau_1) \\ y(t-\tau_2) \\ \vdots \\ y(t-\tau_L) \end{bmatrix}, \tag{4.1}$$

where $\mathbf{p} = [\mathbf{p_1}, \mathbf{p_2}, ..., \mathbf{p_L}]$ and $\tau_\ell = \frac{\mathbf{v}(\theta,\phi)^T\mathbf{p}_\ell}{c}$ is the time delay for the signal to reach the ℓ^{th} sensor with c being the propagation speed of the signal which is prior known deterministic constant.

The value of $\mathbf{v}(\theta, \phi)$ in the time delay equation can defined as,

$$\begin{aligned} \mathbf{v}(\theta,\phi) &= -\begin{bmatrix} v_x(\theta,\phi) \\ v_y(\theta,\phi) \\ v_z(\theta) \end{bmatrix} \\ &= -\begin{bmatrix} \sin(\theta)\cos(\phi) \\ \sin(\theta)\sin(\phi) \\ \cos(\theta) \end{bmatrix}, \end{aligned} \tag{4.2}$$

where $v_x(\theta, \phi)$, $v_y(\theta, \phi)$ and $v_z(\theta)$ denote the direction cosine along x, y and z-axes respectively. The negative sign shows the direction of the incident signal, i.e, the reverse direction from the origin.

Without lose of generality, from the above information, it was clearly deduced that:

$$\begin{aligned} \tau_\ell &= \frac{\mathbf{v}(\theta,\phi)^T p_\ell}{c} \\ &= -\frac{1}{c}\begin{bmatrix} \sin(\theta)\cos(\phi) \\ \sin(\theta)\sin(\phi) \\ \cos(\theta) \end{bmatrix}^{\mathbf{T}} \left[R_{\mathrm{UCA}}\cos\left(\frac{2\pi(\ell-1)}{L_{\mathrm{UCA}}}\right),\ R_{\mathrm{UCA}}\sin\left(\frac{2\pi(\ell-1)}{L_{\mathrm{UCA}}}\right),\ 0\right]^{\mathbf{T}} \\ &= -\frac{1}{c}\left[\sin(\theta)\cos(\phi) \quad \sin(\theta)\sin(\phi) \quad \cos(\phi)\right]\begin{bmatrix} R_{\mathrm{UCA}}\cos\left(\frac{2\pi(\ell-1)}{L_{\mathrm{UCA}}}\right) \\ R_{\mathrm{UCA}}\sin\left(\frac{2\pi(\ell-1)}{L_{\mathrm{UCA}}}\right) \\ 0 \end{bmatrix} \\ &= -\frac{1}{c}\left[\sin(\theta)\cos(\phi)R_{\mathrm{UCA}}\cos\left(\frac{2\pi(\ell-1)}{L_{\mathrm{UCA}}}\right) + \sin(\theta)\sin(\phi)R_{\mathrm{UCA}}\sin\left(\frac{2\pi(\ell-1)}{L_{\mathrm{UCA}}}\right) + 0\right] \\ &= -\frac{R_{\mathrm{UCA}}\sin(\theta)}{c}\left[\cos(\phi)\cos\left(\frac{2\pi(\ell-1)}{L_{\mathrm{UCA}}}\right) + sin(\phi)\sin\left(\frac{2\pi(\ell-1)}{L_{\mathrm{UCA}}}\right)\right] \\ &= -\frac{R_{\mathrm{UCA}}}{c}\sin(\theta)\cos\left(\phi - \frac{2\pi(\ell-1)}{L_{\mathrm{UCA}}}\right). \end{aligned} \tag{4.3}$$

Next, the time domain signals was converted to frequency domain by taking Fourier trans-

form of $\mathbf{y}(t, \mathbf{p})$ from which the ℓ^{th} component was obtained to be;

$$\begin{aligned}
\mathbf{y}_{\ell}(\omega) &= \int_{-\infty}^{\infty} e^{-j\omega t}\mathbf{y}(t - t_{\ell})dt \\
&= \mathbf{y}(\omega)e^{-j\omega t_{\ell}} \\
&= \mathbf{y}(\omega)\exp\left\{j\frac{2\pi f R_{\text{UCA}}}{c}\sin(\theta)\cos\left(\phi - \frac{2\pi(\ell-1)}{L_{\text{UCA}}}\right)\right\} \\
&= \mathbf{y}(\omega)\exp\left\{j2\pi\frac{R_{\text{UCA}}}{\lambda}\sin(\theta)\cos\left(\phi - \frac{2\pi(\ell-1)}{L_{\text{UCA}}}\right)\right\}, \qquad (4.4)
\end{aligned}$$

(by substitution) since $\omega = 2\pi f$ for f being the frequency, $c = \lambda f$; λ is the signal's wavelength and t_{ℓ} is given by equation (4.3). Hence the observations in frequency domain could be written as:

$$\begin{aligned}
\mathbf{y}(\omega) &= \begin{bmatrix} y_{1}(\omega) \\ y_{2}(\omega) \\ \vdots \\ y_{L}(\omega) \end{bmatrix} \\
&= \mathbf{y}(\omega)\begin{bmatrix} \exp\left\{j\frac{2\pi R_{\text{UCA}}}{\lambda}\sin(\theta)\cos(\phi)\right\} \\ \exp\left\{j\frac{2\pi R_{\text{UCA}}}{\lambda}\sin(\theta)\cos\left(\phi - \frac{2\pi}{L_{\text{UCA}}}\right)\right\} \\ \exp\left\{j\frac{2\pi R_{\text{UCA}}}{\lambda}\sin(\theta)\cos\left(\phi - \frac{4\pi}{L_{\text{UCA}}}\right)\right\} \\ \vdots \\ \exp\left\{j\frac{2\pi R_{\text{UCA}}}{\lambda}\sin(\theta)\cos\left(\phi - \frac{2\pi(L_{\text{UCA}}-1)}{L_{\text{UCA}}}\right)\right\} \end{bmatrix}.
\end{aligned}$$

Therefore, the array manifold equals:

$$\mathbf{a}_{\text{UCA}}(\theta, \phi) = \begin{bmatrix} \exp\left\{j\frac{2\pi R_{\text{UCA}}}{\lambda}\sin(\theta)\cos(\phi)\right\} \\ \exp\left\{j\frac{2\pi R_{\text{UCA}}}{\lambda}\sin(\theta)\cos\left(\phi - \frac{2\pi}{L_{\text{UCA}}}\right)\right\} \\ \exp\left\{j\frac{2\pi R_{\text{UCA}}}{\lambda}\sin(\theta)\cos\left(\phi - \frac{4\pi}{L_{\text{UCA}}}\right)\right\} \\ \vdots \\ \exp\left\{j\frac{2\pi R_{\text{UCA}}}{\lambda}\sin(\theta)\cos\left(\phi - \frac{2\pi(L_{\text{UCA}}-1)}{L_{\text{UCA}}}\right)\right\} \end{bmatrix}. \qquad (4.5)$$

where $\theta \in \left[0, \frac{\pi}{2}\right]$, $\phi \in [0, 2\pi)$. In general, the ℓ^{th} entry of $\mathbf{a}_{\text{UCA}}$ was found to be;

$$[\mathbf{a}_{\text{UCA}}(\theta, \phi)]_{\ell} = \exp\left\{j\frac{2\pi R_{\text{UCA}}}{\lambda}\sin(\theta)\cos\left(\phi - \frac{2\pi(\ell-1)}{L_{\text{UCA}}}\right)\right\} \qquad (4.6)$$

for $\ell = 1, 2, 3, \cdots, L_{\text{UCA}}$.

4.1.3 The Concentric Uniform Circular Array (CUCA) Geometry

Two concentric circles of radii R_{in} and R_{out}, both centered at the Cartesian origin and lying on the x-y plane were considered, as shown in Figure 4.2. From figure 4.2 , it was clear

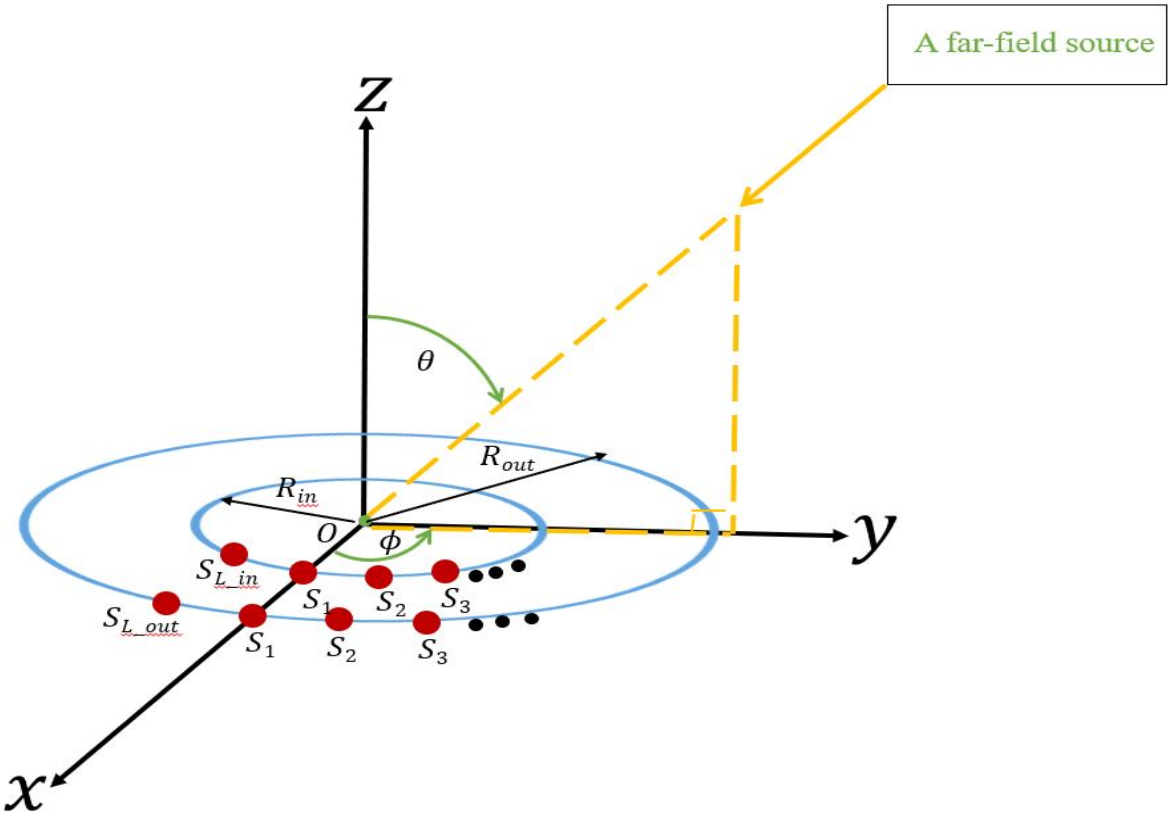

Figure 4.2: A two-circle concentric array.

that the common center of the two concentric circles was fixed and $R_{\text{out}} > R_{\text{in}}$. Since this was true, it followed that $2\pi R_{\text{out}} > 2\pi R_{\text{in}}$. L_{in} and L_{out} were let to denote the number of isotropic sensors placed on the inner and the outer circles' circumference respectively. The location of the array consisting of a set of the isotropic sensors of the concentric circles was denoted by; $S_1, S_2, S_3, \cdots, S_{L_{\text{in}}}$ for the circle of radius R_{in} and $S_1, S_2, S_3, \cdots, S_{L_{\text{out}}}$ for the circle of radius R_{out}.

As seen earlier in the UCA, the waves impinged on the origin at an azimuth angle of ϕ and a polar angle of θ measured counterclockwise and clockwise from the positive x-axis and positive z-axis respectively. The distance between any two adjacent sensors of both circles

was given by; $\frac{2\pi R_{\text{in}}}{L_{\text{in}}}$ and $\frac{2\pi R_{\text{out}}}{L_{\text{out}}}$. Thus the location of the ℓ^{th} sensor was found to be

$$p_\ell \;=\; \begin{cases} \left[R_{\text{in}}\cos\left(\frac{2\pi(\ell_{\text{in}}-1)}{L_{\text{in}}}\right),\; R_{\text{in}}\sin\left(\frac{2\pi(\ell_{\text{in}}-1)}{L_{\text{out}}}\right),\; 0\right]^T, & 1\leq \ell_{\text{in}}\leq L_{\text{in}} \\ \left[R_{\text{out}}\cos\left(\frac{2\pi(\ell_{\text{out}}-1)}{L_{\text{out}}}\right),\; R_{\text{out}}\sin\left(\frac{2\pi(\ell_{\text{out}}-1)}{L_{\text{out}}}\right),\; 0\right]^T, & 1\leq \ell_{\text{out}}\leq L_{\text{out}} \end{cases}.$$

Now, in relation to the already derived array manifold vector for the UCA, the array manifold vector for the CUCA was derived, denoted and defined by

$$\mathbf{a}_{\text{CUCA}} \;=\; \begin{bmatrix} \mathbf{a}_{\text{in}} \\ \mathbf{a}_{\text{out}} \end{bmatrix},$$

where $\mathbf{a}_{\text{in}}$ is the array manifold vector for the circle of radius R_{in} and $\mathbf{a}_{\text{out}}$ is the array manifold vector for the circle of radius R_{out}. Since both $\mathbf{a}_{\text{in}}$ and $\mathbf{a}_{\text{out}}$ were found to depend on the variables (θ,ϕ), then it followed that $\mathbf{a}_{\text{CUCA}}$ denoting the array manifold vector for the CUCA also depended on the θ and ϕ and thus

$$\mathbf{a}_{\text{CUCA}}(\theta,\phi) \;=\; \begin{bmatrix} \mathbf{a}_{\text{in}}(\theta,\phi) \\ \mathbf{a}_{\text{out}}(\theta,\phi) \end{bmatrix}. \tag{4.7}$$

Using equations (4.1), (4.2), (4.3) and (4.4) in the UCA, it was found that the ℓ^{th} entries for $\mathbf{a}_{\text{in}}$ and $\mathbf{a}_{\text{out}}$ were respectively given as,

$$[\mathbf{a}_{\text{in}}(\theta,\phi)]_\ell \;=\; \exp\left\{j\frac{2\pi R_{\text{in}}}{\lambda}\sin(\theta)\cos\left(\phi-\frac{2\pi(\ell_{\text{in}}-1)}{L_{\text{in}}}\right)\right\}$$

for $\ell_{\text{in}}=1,2,3,\cdots,L_{\text{in}}$ and

$$[\mathbf{a}_{\text{out}}(\theta,\phi)]_\ell \;=\; \exp\left\{j\frac{2\pi R_{\text{out}}}{\lambda}\sin(\theta)\cos\left(\phi-\frac{2\pi(\ell_{\text{out}}-1)}{L_{\text{out}}}\right)\right\}$$

for $\ell_{\text{out}}=1,2,3,\cdots,L_{\text{out}}$, which were respectively expanded to yield

$$\mathbf{a}_{\text{in}}(\theta,\phi) \;=\; \begin{bmatrix} \exp\left\{j\frac{2\pi R_{\text{in}}}{\lambda}\sin(\theta)\cos(\phi)\right\} \\ \exp\left\{j\frac{2\pi R_{\text{in}}}{\lambda}\sin(\theta)\cos\left(\phi-\frac{2\pi}{L_{\text{in}}}\right)\right\} \\ \exp\left\{j\frac{2\pi R_{\text{in}}}{\lambda}\sin(\theta)\cos\left(\phi-\frac{4\pi}{L_{\text{in}}}\right)\right\} \\ \vdots \\ \exp\left\{j\frac{2\pi R_{\text{in}}}{\lambda}\sin(\theta)\cos\left(\phi-\frac{2\pi(L_{\text{in}}-1)}{L_{\text{in}}}\right)\right\} \end{bmatrix}, \tag{4.8}$$

and

$$\mathbf{a}_{\text{out}}(\theta,\phi) = \begin{bmatrix} \exp\left\{j\frac{2\pi R_{\text{out}}}{\lambda}\sin(\theta)\cos(\phi)\right\} \\ \exp\left\{j\frac{2\pi R_{\text{out}}}{\lambda}\sin(\theta)\cos\left(\phi-\frac{2\pi}{L_{\text{out}}}\right)\right\} \\ \exp\left\{j\frac{2\pi R_{\text{out}}}{\lambda}\sin(\theta)\cos\left(\phi-\frac{4\pi}{L_{\text{out}}}\right)\right\} \\ \vdots \\ \exp\left\{j\frac{2\pi R_{\text{out}}}{\lambda}\sin(\theta)\cos\left(\phi-\frac{2\pi(L_{\text{out}}-1)}{L_{\text{out}}}\right)\right\} \end{bmatrix}. \tag{4.9}$$

Hence inserting (4.8)-(4.9) in (4.7), the array manifold vector for the CUCA is given by,

$$\mathbf{a}_{\text{CUCA}}(\theta,\phi) = \begin{bmatrix} \exp\left\{j\frac{2\pi R_{\text{in}}}{\lambda}\sin(\theta)\cos(\phi)\right\} \\ \exp\left\{j\frac{2\pi R_{\text{in}}}{\lambda}\sin(\theta)\cos\left(\phi-\frac{2\pi}{L_{\text{in}}}\right)\right\} \\ \exp\left\{j\frac{2\pi R_{\text{in}}}{\lambda}\sin(\theta)\cos\left(\phi-\frac{4\pi}{L_{\text{in}}}\right)\right\} \\ \vdots \\ \exp\left\{j\frac{2\pi R_{\text{in}}}{\lambda}\sin(\theta)\cos\left(\phi-\frac{2\pi(L_{\text{in}}-1)}{L_{\text{in}}}\right)\right\} \\ \exp\left\{j\frac{2\pi R_{\text{out}}}{\lambda}\sin(\theta)\cos(\phi)\right\} \\ \exp\left\{j\frac{2\pi R_{\text{out}}}{\lambda}\sin(\theta)\cos\left(\phi-\frac{2\pi}{L_{\text{out}}}\right)\right\} \\ \exp\left\{j\frac{2\pi R_{\text{out}}}{\lambda}\sin(\theta)\cos\left(\phi-\frac{4\pi}{L_{\text{out}}}\right)\right\} \\ \vdots \\ \exp\left\{j\frac{2\pi R_{\text{out}}}{\lambda}\sin(\theta)\cos\left(\phi-\frac{2\pi(L_{\text{out}}-1)}{L_{\text{out}}}\right)\right\} \end{bmatrix}. \tag{4.10}$$

In general, the ℓ^{th} entry of $[\mathbf{a}_{\text{CUCA}}(\theta,\phi)]$ can be expressed as,

$$[\mathbf{a}_{\text{CUCA}}(\theta,\phi)]_{\ell} = \begin{cases} \exp\left\{j\frac{2\pi R_{\text{in}}}{\lambda}\sin(\theta)\cos\left(\phi-\frac{2\pi(\ell_{\text{in}}-1)}{L_{\text{in}}}\right)\right\}, & 1\le\ell_{\text{in}}\le L_{\text{in}} \\ \exp\left\{j\frac{2\pi R_{\text{out}}}{\lambda}\sin(\theta)\cos\left(\phi-\frac{2\pi(\ell_{\text{out}}-1)}{L_{\text{out}}}\right)\right\}, & 1\le\ell_{\text{out}}\le L_{\text{out}} \end{cases}.$$

4.2 The Cramér-Rao Bound (CRB) Derivation

This section presents the derivation of the Cramér-Rao Bound for the 2-circle concentric uniform array geometry. Consequently, the Cramér-Rao Bound for the uniform circular array geometry is stated.

4.2.1 The Statistical Data Model:

Suppose the data was corrupted by additive noise. Then, the observed data vector can be expressed as

$$\mathbf{x}(m) \;=\; \mathbf{a}(\theta,\phi)s(m) + \mathbf{n}(m), \tag{4.11}$$

where, $s(m)$ is the signal received at time instant m and $\mathbf{n}(m)$ is additive complex-valued spatio-temporal white Gaussian noise with prior known mean of zero and variance of σ_n^2 [38, 35, 37, 36, 33, 13, 14, 25, 23, 22, 19, 34, 5, 28, 21]. M number of discrete-time samples were considered, and thus (4.11) was represented as

$$\mathbf{x} \;=\; \mathbf{s}\otimes\mathbf{a}(\theta,\phi) + \mathbf{n}, \tag{4.12}$$

where

$$\begin{aligned}
\mathbf{x} &:= \left[\mathbf{x}^T(1),\ \mathbf{x}^T(2),\ \mathbf{x}^T(3),\cdots,\mathbf{x}^T(M)\right]^T,\\
\mathbf{s} &:= \left[s(1),\ s(2),\ s(3),\cdots,s(M)\right]^T,\\
\mathbf{n} &:= \left[\mathbf{n}^T(1),\ \mathbf{n}^T(2),\ \mathbf{n}^T(3),\cdots,\mathbf{n}^T(M)\right]^T,
\end{aligned}$$

denote the observations, the signals, and the additive noise, respectively. Moreover, $\otimes$ and ^{T}, denote the Kronecker product and the transposition, respectively [36, 38, 37, 33].

4.2.2 The Probability Distribution Function (PDF) of the Data

As a consequent of the observed data being in vector form, then the data's probability distribution function (PDF) was deduced to be,

$$p(\mathbf{x}|\theta,\phi) = \frac{1}{\sqrt{|2\pi\mathbf{\Gamma}(\theta,\phi)|}}\left\{-\frac{1}{2}\left[\mathbf{x}-\boldsymbol{\mu}(\theta,\phi)\right]^H\mathbf{\Gamma}(\theta,\phi)^{-1}\left[\mathbf{x}-\boldsymbol{\mu}(\theta,\phi)\right]\right\} \quad (4.13)$$

where

$$\begin{aligned}\boldsymbol{\mu}(\theta,\phi) &:= E[\mathbf{x}] \\ &= \mathbf{s}\otimes\mathbf{a}(\theta,\phi), \quad (4.14)\\ \mathbf{\Gamma}(\theta,\phi) &:= E\left\{[\mathbf{x}-\boldsymbol{\mu}(\theta,\phi)][\mathbf{x}-\boldsymbol{\mu}(\theta,\phi)]^H\right\} \\ &= \sigma_n^2\mathbf{I}_{(L_{\text{in}}+L_{\text{out}})M}, \quad (4.15)\end{aligned}$$

for $\boldsymbol{\mu}(\theta,\phi)$ and $\mathbf{\Gamma}(\theta,\phi)$ being the mean vector and the covariance matrix of the observed data vector respectively and $\mathbf{I}_{(L_{\text{in}}+L_{\text{out}})M}$ denotes an identity matrix of size $(L_{\text{in}}+L_{\text{out}})M\times(L_{\text{in}}+L_{\text{out}})M$.

4.2.3 The Fisher Information Matrix (FIM)

It was recalled that the observed data vector was complex-valued and therefore, the Fisher information matrix (FIM) had a $(k,n)^{th}$ entry of,

$$[\mathbf{F}(\xi)]_{k,n} = 2\text{Re}\left\{\left[\frac{\partial\boldsymbol{\mu}}{\partial\xi_k}\right]^H\mathbf{\Gamma}^{-1}\frac{\partial\boldsymbol{\mu}}{\partial\xi_n}\right\}+\text{Tr}\left\{\mathbf{\Gamma}^{-1}\frac{\partial\mathbf{\Gamma}}{\partial\xi_k}\mathbf{\Gamma}^{-1}\frac{\partial\mathbf{\Gamma}}{\partial\xi_n}\right\}\ , \quad (4.16)$$

where ξ_n refers to the n^{th} entry of $\boldsymbol{\xi}$, $\boldsymbol{\xi}=\{\theta,\phi\}$ is the set of the unknown but deterministic parameters to be estimated, $\text{Re}\{\cdot\}$ symbolizes the real-valued part of the entity inside the curly brackets, $\text{Tr}\{\cdot\}$ represents the trace of the contents inside the curly brackets, and ^{H} denotes conjugate transposition [38, 35, 37, 33].

From equation (4.15),

$$\begin{aligned}\frac{\partial\mathbf{\Gamma}}{\partial\xi_k} &= \frac{\partial\mathbf{\Gamma}}{\partial\xi_n} \\ &= 0\ ,\end{aligned}$$

implying that the second term of equation (4.16) vanishes. Inserting (4.15) in (4.16) yielded:

$$\begin{aligned}\left[\mathbf{F}(\xi)\right]_{k,n} &= 2\mathrm{Re}\left\{\left[\frac{\partial\boldsymbol{\mu}}{\partial\xi_k}\right]^H \boldsymbol{\Gamma}^{-1}\frac{\partial\boldsymbol{\mu}}{\partial\xi_n}\right\} \\ &= \frac{2}{\sigma_n^2}\mathrm{Re}\left\{\left[\frac{\partial\boldsymbol{\mu}}{\partial\xi_k}\right]^H \frac{\partial\boldsymbol{\mu}}{\partial\xi_n}\right\} \quad . \end{aligned} \tag{4.17}$$

With equation (4.12) it was found that,

$$\begin{aligned}\left[\frac{\partial\boldsymbol{\mu}}{\partial\xi_k}\right]^H \frac{\partial\boldsymbol{\mu}}{\partial\xi_n} &= \left[\mathbf{s}\otimes\frac{\partial\mathbf{a}(\theta,\phi)}{\partial\xi_k}\right]^H \left[\mathbf{s}\otimes\frac{\partial\mathbf{a}(\theta,\phi)}{\partial\xi_\mathbf{n}}\right] \\ &= \mathbf{s}^H\mathbf{s}\left\{\left[\frac{\partial\mathbf{a}(\theta,\phi)}{\partial\xi_k}\right]^H \left[\frac{\partial\mathbf{a}(\theta,\phi)}{\partial\xi_n}\right]\right\} \quad , \end{aligned} \tag{4.18}$$

since $\mathbf{s}$ for the signal was complex-valued sinusoid and $\boldsymbol{\mu}(\theta,\phi)$ depended explicitly on θ and ϕ.

Substituting equation (4.18) in equation (4.17):

$$\left[\mathbf{F}(\xi)\right]_{k,n} = \frac{2}{\sigma_n^2}\mathbf{s}^H\mathbf{s}\left\{\mathrm{Re}\left[\frac{\partial\mathbf{a}(\theta,\phi)}{\partial\xi_k}\right]^H \left[\frac{\partial\mathbf{a}(\theta,\phi)}{\partial\xi_n}\right]\right\} . \tag{4.19}$$

Here, the FIM was a 2×2 matrix because the parameters to be estimated were two i.e θ and ϕ. Hence,

$$\mathbf{F}(\boldsymbol{\xi}) = \begin{bmatrix} F_{\theta,\theta} & F_{\theta,\phi} \\ F_{\phi,\theta} & F_{\phi,\phi}\end{bmatrix}, \tag{4.20}$$

from which

$$\begin{bmatrix}\mathrm{CRB}(\theta) & * \\ * & \mathrm{CRB}(\phi)\end{bmatrix} = \begin{bmatrix} F_{\theta,\theta} & F_{\theta,\phi} \\ F_{\phi,\theta} & F_{\phi,\phi}\end{bmatrix}^{-1}, \tag{4.21}$$

where $*$ denotes elements not of interest for the present purpose. From (4.21):

$$F_{\theta,\theta} = 2\frac{\mathbf{s}^H\mathbf{s}}{\sigma_n^2}\mathrm{Re}\left\{\left[\frac{\partial\mathbf{a}(\theta,\phi)}{\partial\theta}\right]^H \left[\frac{\partial\mathbf{a}(\theta,\phi)}{\partial\theta}\right]\right\}, \tag{4.22}$$

$$F_{_{\theta,\phi}} = 2\frac{\mathbf{s}^H\mathbf{s}}{\sigma_n^2}\mathrm{Re}\left\{\left[\frac{\partial\mathbf{a}(\theta,\phi)}{\partial\theta}\right]^H\left[\frac{\partial\mathbf{a}(\theta,\phi)}{\partial\phi}\right]\right\}, \tag{4.23}$$

$$F_{_{\phi,\theta}} = 2\frac{\mathbf{s}^H\mathbf{s}}{\sigma_n^2}\mathrm{Re}\left\{\left[\frac{\partial\mathbf{a}(\theta,\phi)}{\partial\phi}\right]^H\left[\frac{\partial\mathbf{a}(\theta,\phi)}{\partial\theta}\right]\right\}, \tag{4.24}$$

and

$$F_{_{\phi,\phi}} = 2\frac{\mathbf{s}^H\mathbf{s}}{\sigma_n^2}\mathrm{Re}\left\{\left[\frac{\partial\mathbf{a}(\theta,\phi)}{\partial\phi}\right]^H\left[\frac{\partial\mathbf{a}(\theta,\phi)}{\partial\phi}\right]\right\}. \tag{4.25}$$

4.2.4 The Signal

Since $\mathbf{s}$ for the signal was complex-valued, then it was defined as $s(m) = \sigma_s \exp\{j(2\pi fm + \varphi)\}$ for $m = 1, 2, 3, \cdots, M$; where φ denotes the signal phase. The $s(m)$ was expanded as

$$\mathbf{s} = \sigma_s \begin{bmatrix} e^{j(2\pi f+\varphi)} \\ e^{j(4\pi f+\varphi)} \\ e^{j(6\pi f+\varphi)} \\ \vdots \\ e^{j(2M\pi f+\varphi)} \end{bmatrix}.$$

Therefore, the value of $\mathbf{s}^H\mathbf{s}$ was found as follows:

$$\begin{aligned} \mathbf{s}^H\mathbf{s} &= \sigma_s^2 \begin{bmatrix} e^{-j(2\pi f+\varphi)} \\ e^{-j(4\pi f+\varphi)} \\ e^{-j(6\pi f+\varphi)} \\ \vdots \\ e^{-j(2M\pi f+\varphi)} \end{bmatrix}^T \begin{bmatrix} e^{j(2\pi f+\varphi)} \\ e^{j(4\pi f+\varphi)} \\ e^{j(6\pi f+\varphi)} \\ \vdots \\ e^{j(2M\pi f+\varphi)} \end{bmatrix} \\ &= \sigma_s^2 \underbrace{[1+1+1+\cdots+1]}_{\text{M times}} \\ &= M\sigma_s^2 . \end{aligned} \tag{4.26}$$

4.2.5 Expansion of the FIM Elements

Next the values of $F_{\theta,\theta}$, $F_{\theta,\phi}$ = $F_{\phi,\theta}$, and $F_{\phi,\phi}$ were computed as follows:

Using equation (4.22)

$$
\begin{aligned}
\left[\frac{\partial \mathbf{a}(\theta,\phi)}{\partial \theta}\right]^H \left[\frac{\partial \mathbf{a}(\theta,\phi)}{\partial \theta}\right] &= \begin{bmatrix}
\left(\frac{2\pi R_{\text{in}}}{\lambda}\right)^2 \cos^2(\theta)\cos^2(\phi) \\
\left(\frac{2\pi R_{\text{in}}}{\lambda}\right)^2 \cos^2(\theta)\cos^2\left(\phi - \frac{2\pi}{L_{\text{in}}}\right) \\
\left(\frac{2\pi R_{\text{in}}}{\lambda}\right)^2 \cos^2(\theta)\cos^2\left(\phi - \frac{4\pi}{L_{\text{in}}}\right) \\
\vdots \\
\left(\frac{2\pi R_{\text{in}}}{\lambda}\right)^2 \cos^2(\theta)\cos^2\left(\phi - \frac{2\pi(L_{\text{in}}-1)}{L_{\text{in}}}\right) \\
\left(\frac{2\pi R_{\text{out}}}{\lambda}\right)^2 \cos^2(\theta)\cos^2(\phi) \\
\left(\frac{2\pi R_{\text{out}}}{\lambda}\right)^2 \cos^2(\theta)\cos^2\left(\phi - \frac{2\pi}{L_{\text{out}}}\right) \\
\left(\frac{2\pi R_{\text{out}}}{\lambda}\right)^2 \cos^2(\theta)\cos^2\left(\phi - \frac{4\pi}{L_{\text{out}}}\right) \\
\vdots \\
\left(\frac{2\pi R_{\text{out}}}{\lambda}\right)^2 \cos^2(\theta)\cos^2\left(\phi - \frac{2\pi(L_{\text{out}}-1)}{L_{\text{out}}}\right)
\end{bmatrix} \\
&\odot \left\{ \begin{bmatrix}
e^{-j\frac{2\pi R_{\text{in}}}{\lambda}\sin(\theta)\cos(\phi)} \\
e^{-j\frac{2\pi R_{\text{in}}}{\lambda}\sin(\theta)\cos\left(\phi - \frac{2\pi}{L_{\text{in}}}\right)} \\
e^{-j\frac{2\pi R_{\text{in}}}{\lambda}\sin(\theta)\cos\left(\phi - \frac{4\pi}{L_{\text{in}}}\right)} \\
\vdots \\
e^{-j\frac{2\pi R_{\text{in}}}{\lambda}\sin(\theta)\cos\left(\phi - \frac{2\pi(L_{\text{in}}-1)}{L_{\text{in}}}\right)} \\
e^{-j\frac{2\pi R_{\text{out}}}{\lambda}\sin(\theta)\cos(\phi)} \\
e^{-j\frac{2\pi R_{\text{out}}}{\lambda}\sin(\theta)\cos\left(\phi - \frac{2\pi}{L_{\text{out}}}\right)} \\
e^{-j\frac{2\pi R_{\text{out}}}{\lambda}\sin(\theta)\cos\left(\phi - \frac{4\pi}{L_{\text{out}}}\right)} \\
\vdots \\
e^{-j\frac{2\pi R_{\text{out}}}{\lambda}\sin(\theta)\cos\left(\phi - \frac{2\pi(L_{\text{out}}-1)}{L_{\text{out}}}\right)}
\end{bmatrix}^{\mathrm{T}} \begin{bmatrix}
e^{j\frac{2\pi R_{\text{in}}}{\lambda}\sin(\theta)\cos(\phi)} \\
e^{j\frac{2\pi R_{\text{in}}}{\lambda}\sin(\theta)\cos\left(\phi - \frac{2\pi}{L_{\text{in}}}\right)} \\
e^{j\frac{2\pi R_{\text{in}}}{\lambda}\sin(\theta)\cos\left(\phi - \frac{4\pi}{L_{\text{in}}}\right)} \\
\vdots \\
e^{j\frac{2\pi R_{\text{in}}}{\lambda}\sin(\theta)\cos\left(\phi - \frac{2\pi(L_{\text{in}}-1)}{L_{\text{in}}}\right)} \\
e^{j\frac{2\pi R_{\text{out}}}{\lambda}\sin(\theta)\cos(\phi)} \\
e^{j\frac{2\pi R_{\text{out}}}{\lambda}\sin(\theta)\cos\left(\phi - \frac{2\pi}{L_{\text{out}}}\right)} \\
e^{j\frac{2\pi R_{\text{out}}}{\lambda}\sin(\theta)\cos\left(\phi - \frac{4\pi}{L_{\text{out}}}\right)} \\
\vdots \\
e^{j\frac{2\pi R_{\text{out}}}{\lambda}\sin(\theta)\cos\left(\phi - \frac{2\pi(L_{\text{out}}-1)}{L_{\text{out}}}\right)}
\end{bmatrix} \right\} \\
&= \left(\frac{2\pi R_{\text{in}}}{\lambda}\cos(\theta)\right)^2 \underbrace{\sum_{\ell_{\text{in}}=1}^{L_{\text{in}}} \cos^2\left(\phi - \frac{2\pi(\ell_{\text{in}}-1)}{L_{\text{in}}}\right)}_{:=\, L_{\text{in}}/2} \\
&\quad + \left(\frac{2\pi R_{\text{out}}}{\lambda}\cos(\theta)\right)^2 \underbrace{\sum_{\ell_{\text{out}}=1}^{L_{\text{out}}} \cos^2\left(\phi - \frac{2\pi(\ell_{\text{out}}-1)}{L_{\text{out}}}\right)}_{:=\, L_{\text{out}}/2} \\
&= \left(\frac{2\pi R_{\text{in}}}{\lambda}\cos(\theta)\right)^2 \frac{L_{\text{in}}}{2} + \left(\frac{2\pi R_{\text{out}}}{\lambda}\cos(\theta)\right)^2 \frac{L_{\text{out}}}{2}. \qquad (4.27)
\end{aligned}
$$

In the above, $\odot$ is the Hadamard product.

Using (4.27) in (4.22) we obtain,

$$F_{\theta,\theta} \;=\; 4M\left(\frac{\pi}{\lambda}\frac{\sigma_s}{\sigma_n}\right)^2\left(R_{\rm in}^2 L_{\rm in} + R_{\rm out}^2 L_{\rm out}\right)\cos^2(\theta)\;. \tag{4.28}$$

Using (4.25):

$$
\begin{aligned}
\left[\frac{\partial \mathbf{a}(\theta,\phi)}{\partial \phi}\right]^H \left[\frac{\partial \mathbf{a}(\theta,\phi)}{\partial \phi}\right] &= \begin{bmatrix}
\left(\frac{2\pi R_{\text{in}}}{\lambda}\right)^2 \sin^2(\theta)\sin^2(\phi) \\
\left(\frac{2\pi R_{\text{in}}}{\lambda}\right)^2 \sin^2(\theta)\sin^2\left(\phi-\frac{2\pi}{L_{\text{in}}}\right) \\
\left(\frac{2\pi R_{\text{in}}}{\lambda}\right)^2 \sin^2(\theta)\sin^2\left(\phi-\frac{4\pi}{L_{\text{in}}}\right) \\
\vdots \\
\left(\frac{2\pi R_{\text{in}}}{\lambda}\right)^2 \sin^2(\theta)\sin^2\left(\phi-\frac{2\pi(L_{\text{in}}-1)}{L_{\text{in}}}\right) \\
\left(\frac{2\pi R_{\text{out}}}{\lambda}\right)^2 \sin^2(\theta)\sin^2(\phi) \\
\left(\frac{2\pi R_{\text{out}}}{\lambda}\right)^2 \sin^2(\theta)\sin^2\left(\phi-\frac{2\pi}{L_{\text{out}}}\right) \\
\left(\frac{2\pi R_{\text{out}}}{\lambda}\right)^2 \sin^2(\theta)\sin^2\left(\phi-\frac{4\pi}{L_{\text{out}}}\right) \\
\vdots \\
\left(\frac{2\pi R_{\text{out}}}{\lambda}\right)^2 \cos^2(\theta)\cos^2\left(\phi-\frac{2\pi(L_{\text{out}}-1)}{L_{\text{out}}}\right)
\end{bmatrix} \\
&\quad \odot \left\{ \begin{bmatrix}
e^{-j\frac{2\pi R_{\text{in}}}{\lambda}\sin(\theta)\cos(\phi)} \\
e^{-j\frac{2\pi R_{\text{in}}}{\lambda}\sin(\theta)\cos\left(\phi-\frac{2\pi}{L_{\text{in}}}\right)} \\
e^{-j\frac{2\pi R_{\text{in}}}{\lambda}\sin(\theta)\cos\left(\phi-\frac{4\pi}{L_{\text{in}}}\right)} \\
\vdots \\
e^{-j\frac{2\pi R_{\text{in}}}{\lambda}\sin(\theta)\cos\left(\phi-\frac{2\pi(L_{\text{in}}-1)}{L_{\text{in}}}\right)} \\
e^{-j\frac{2\pi R_{\text{out}}}{\lambda}\sin(\theta)\cos(\phi)} \\
e^{-j\frac{2\pi R_{\text{out}}}{\lambda}\sin(\theta)\cos\left(\phi-\frac{2\pi}{L_{\text{out}}}\right)} \\
e^{-j\frac{2\pi R_{\text{out}}}{\lambda}\sin(\theta)\cos\left(\phi-\frac{4\pi}{L_{\text{out}}}\right)} \\
\vdots \\
e^{-j\frac{2\pi R_{\text{out}}}{\lambda}\sin(\theta)\cos\left(\phi-\frac{2\pi(L_{\text{out}}-1)}{L_{\text{out}}}\right)}
\end{bmatrix}^{\text{T}} \begin{bmatrix}
e^{j\frac{2\pi R_{\text{in}}}{\lambda}\sin(\theta)\cos(\phi)} \\
e^{j\frac{2\pi R_{\text{in}}}{\lambda}\sin(\theta)\cos\left(\phi-\frac{2\pi}{L_{\text{in}}}\right)} \\
e^{j\frac{2\pi R_{\text{in}}}{\lambda}\sin(\theta)\cos\left(\phi-\frac{4\pi}{L_{\text{in}}}\right)} \\
\vdots \\
e^{j\frac{2\pi R_{\text{in}}}{\lambda}\sin(\theta)\cos\left(\phi-\frac{2\pi(L_{\text{in}}-1)}{L_{\text{in}}}\right)} \\
e^{j\frac{2\pi R_{\text{out}}}{\lambda}\sin(\theta)\cos(\phi)} \\
e^{j\frac{2\pi R_{\text{out}}}{\lambda}\sin(\theta)\cos\left(\phi-\frac{2\pi}{L_{\text{out}}}\right)} \\
e^{j\frac{2\pi R_{\text{out}}}{\lambda}\sin(\theta)\cos\left(\phi-\frac{4\pi}{L_{\text{out}}}\right)} \\
\vdots \\
e^{j\frac{2\pi R_{\text{out}}}{\lambda}\sin(\theta)\cos\left(\phi-\frac{2\pi(L_{\text{out}}-1)}{L_{\text{out}}}\right)}
\end{bmatrix} \right\} \\
&= \left(\frac{2\pi R_{\text{in}}}{\lambda}\sin(\theta)\right)^2 \underbrace{\sum_{\ell_{\text{in}}=1}^{L_{\text{in}}} \sin^2\left(\phi-\frac{2\pi(\ell_{\text{in}}-1)}{L_{\text{in}}}\right)}_{:=\, L_{\text{in}}/2} \\
&\quad + \left(\frac{2\pi R_{\text{out}}}{\lambda}\sin(\theta)\right)^2 \underbrace{\sum_{\ell_{\text{out}}=1}^{L_{\text{out}}} \sin^2\left(\phi-\frac{2\pi(\ell_{\text{out}}-1)}{L_{\text{out}}}\right)}_{:=\, L_{\text{out}}/2} \\
&= \left(\frac{2\pi R_{\text{in}}}{\lambda}\sin(\theta)\right)^2 \frac{L_{\text{in}}}{2} + \left(\frac{2\pi R_{\text{out}}}{\lambda}\sin(\theta)\right)^2 \frac{L_{\text{out}}}{2}\,. \qquad (4.29)
\end{aligned}
$$

Therefore, Using (4.29) in (4.25):

$$
F_{\phi,\phi} = 4M\left(\frac{\pi}{\lambda}\frac{\sigma_s}{\sigma_n}\right)^2 \left(R_{\text{in}}^2 L_{\text{in}} + R_{\text{out}}^2 L_{\text{out}}\right)\sin^2(\theta). \qquad (4.30)
$$

Using equation (4.23) which is equivalent to equation (4.24) we obtain,

$$
\begin{aligned}
&\left[\frac{\partial \mathbf{a}(\theta,\phi)}{\partial \theta}\right]^H \left[\frac{\partial \mathbf{a}(\theta,\phi)}{\partial \phi}\right] \\
&= \left\{\begin{bmatrix}
j\frac{2\pi R_{\text{in}}}{\lambda}\cos(\theta)\cos(\phi) \\
j\frac{2\pi R_{\text{in}}}{\lambda}\cos(\theta)\cos\left(\phi-\frac{2\pi}{L_{\text{in}}}\right) \\
j\frac{2\pi R_{\text{in}}}{\lambda}\cos(\theta)\cos\left(\phi-\frac{4\pi}{L_{\text{in}}}\right) \\
\vdots \\
j\frac{2\pi R_{\text{in}}}{\lambda}\cos(\theta)\cos\left(\phi-\frac{2\pi(L_{\text{in}}-1)}{L_{\text{in}}}\right) \\
j\frac{2\pi R_{\text{out}}}{\lambda}\cos(\theta)\cos(\phi) \\
j\frac{2\pi R_{\text{out}}}{\lambda}\cos(\theta)\cos\left(\phi-\frac{2\pi}{L_{\text{out}}}\right) \\
j\frac{2\pi R_{\text{out}}}{\lambda}\cos(\theta)\cos\left(\phi-\frac{4\pi}{L_{\text{out}}}\right) \\
\vdots \\
j\frac{2\pi R_{\text{out}}}{\lambda}\cos^2(\theta)\cos^2\left(\phi-\frac{2\pi(L_{\text{out}}-1)}{L_{\text{out}}}\right)
\end{bmatrix} \odot \begin{bmatrix}
e^{-j\frac{2\pi R_{\text{in}}}{\lambda}\sin(\theta)\cos(\phi)} \\
e^{-j\frac{2\pi R_{\text{in}}}{\lambda}\sin(\theta)\cos\left(\phi-\frac{2\pi}{L_{\text{in}}}\right)} \\
e^{-j\frac{2\pi R_{\text{in}}}{\lambda}\sin(\theta)\cos\left(\phi-\frac{4\pi}{L_{\text{in}}}\right)} \\
\vdots \\
e^{-j\frac{2\pi R_{\text{in}}}{\lambda}\sin(\theta)\cos\left(\phi-\frac{2\pi(L_{\text{in}}-1)}{L_{\text{in}}}\right)} \\
e^{-j\frac{2\pi R_{\text{out}}}{\lambda}\sin(\theta)\cos(\phi)} \\
e^{-j\frac{2\pi R_{\text{out}}}{\lambda}\sin(\theta)\cos\left(\phi-\frac{2\pi}{L_{\text{out}}}\right)} \\
e^{-j\frac{2\pi R_{\text{out}}}{\lambda}\sin(\theta)\cos\left(\phi-\frac{4\pi}{L_{\text{out}}}\right)} \\
\vdots \\
e^{-j\frac{2\pi R_{\text{out}}}{\lambda}\sin(\theta)\cos\left(\phi-\frac{2\pi(L_{\text{out}}-1)}{L_{\text{out}}}\right)}
\end{bmatrix}^{\text{T}}\right\} \\
&\times \left\{\begin{bmatrix}
-j\frac{2\pi R_{\text{in}}}{\lambda}\sin(\theta)\sin(\phi) \\
-j\frac{2\pi f R_{\text{in}}}{\lambda}\sin(\theta)\sin\left(\phi-\frac{2\pi}{L_{\text{in}}}\right) \\
-j\frac{2\pi R_{\text{in}}}{\lambda}\sin(\theta)\sin\left(\phi-\frac{4\pi}{L_{\text{in}}}\right) \\
\vdots \\
-j\frac{2\pi R_{\text{in}}}{\lambda}\sin(\theta)\sin\left(\phi-\frac{2\pi(L_{\text{in}}-1)}{L_{\text{in}}}\right) \\
-j\frac{2\pi R_{\text{out}}}{\lambda}\sin(\theta)\sin(\phi) \\
-j\frac{2\pi R_{\text{out}}}{\lambda}\sin(\theta)\sin\left(\phi-\frac{2\pi}{L_{\text{out}}}\right) \\
-j\frac{2\pi R_{\text{out}}}{\lambda}\sin(\theta)\sin\left(\phi-\frac{4\pi}{L_{\text{out}}}\right) \\
\vdots \\
-j\frac{2\pi R_{\text{out}}}{\lambda}\cos(\theta)\cos^2\left(\phi-\frac{2\pi(L_{\text{out}}-1)}{L_{\text{out}}}\right)
\end{bmatrix} \odot \begin{bmatrix}
e^{j\frac{2\pi R_{\text{in}}}{\lambda}\sin(\theta)\cos(\phi)} \\
e^{j\frac{2\pi R_{\text{in}}}{\lambda}\sin(\theta)\cos\left(\phi-\frac{2\pi}{L_{\text{in}}}\right)} \\
e^{j\frac{2\pi R_{\text{in}}}{\lambda}\sin(\theta)\cos\left(\phi-\frac{4\pi}{L_{\text{in}}}\right)} \\
\vdots \\
e^{j\frac{2\pi R_{\text{in}}}{\lambda}\sin(\theta)\cos\left(\phi-\frac{2\pi(L_{\text{in}}-1)}{L_{\text{in}}}\right)} \\
e^{j\frac{2\pi R_{\text{out}}}{\lambda}\sin(\theta)\cos(\phi)} \\
e^{j\frac{2\pi R_{\text{out}}}{\lambda}\sin(\theta)\cos\left(\phi-\frac{2\pi}{L_{\text{out}}}\right)} \\
e^{j\frac{2\pi R_{\text{out}}}{\lambda}\sin(\theta)\cos\left(\phi-\frac{4\pi}{L_{\text{out}}}\right)} \\
\vdots \\
e^{j\frac{2\pi f R_{\text{out}}}{\lambda}\sin(\theta)\cos\left(\phi-\frac{2\pi(L_{\text{out}}-1)}{L_{\text{out}}}\right)}
\end{bmatrix}\right\} \\
&= \left(\frac{2\pi R_{\text{in}}}{\lambda}\right)^2\frac{\sin 2\theta}{4}\underbrace{\sum_{\ell_{\text{in}}=1}^{L_{\text{in}}}\sin\left(2\phi-\frac{2\pi(\ell_{\text{in}}-1)}{L_{\text{in}}}\right)}_{:=\,0} \\
&\quad +\left(\frac{2\pi R_{\text{out}}}{\lambda}\right)^2\frac{\sin 2\theta}{4}\underbrace{\sum_{\ell_{\text{out}}=1}^{L_{\text{out}}}\sin\left(2\phi-\frac{2\pi(\ell_{\text{out}}-1)}{L_{\text{out}}}\right)}_{:=\,0} \\
&= 0\,. \qquad (4.31)
\end{aligned}
$$

Hence, Using (4.31) in (4.24) it was discovered that,

$$\begin{aligned} F_{\theta,\phi} &= F_{\phi,\theta} \\ &= 0\,. \end{aligned} \tag{4.32}$$

4.2.6 Formulation of the $\mathrm{CRB}(\theta)$ and $\mathrm{CRB}(\phi)$ from the FIM

Using equation (4.21), $\mathrm{CRB}_{\mathrm{CUCA}}(\theta)$ and $\mathrm{CRB}_{\mathrm{CUCA}}(\phi)$ were computed as follows:

$$\begin{bmatrix} \mathrm{CRB}_{\mathrm{CUCA}}(\theta) & * \\ * & \mathrm{CRB}_{\mathrm{CUCA}}(\phi) \end{bmatrix} = \begin{bmatrix} F_{\theta,\theta} & 0 \\ 0 & F_{\phi,\phi} \end{bmatrix}^{-1} \tag{4.33}$$

Hence using (4.33) above it was discovered that,

$$\begin{aligned} \mathrm{CRB}_{\mathrm{CUCA}}(\theta) &= F^{-1}_{\phi,\phi} \\ &= \frac{1}{4M\frac{\sigma_s^2}{\sigma_n^2}\left(R_{\mathrm{in}}^2 L_{\mathrm{in}} + R_{\mathrm{out}}^2 L_{\mathrm{out}}\right)\left(\frac{\pi}{\lambda}\cos(\theta)\right)^2} \\ &= \frac{1}{4\pi^2}\frac{1}{M}\frac{\lambda^2}{R_{\mathrm{in}}^2 L_{\mathrm{in}} + R_{\mathrm{out}}^2 L_{\mathrm{out}}}\left(\frac{\sigma_n}{\sigma_s}\right)^2 \sec^2(\theta) \\ &= \frac{1}{4\pi^2}\frac{1}{M}\left[\frac{R_{\mathrm{in}}^2}{\lambda^2}L_{\mathrm{in}} + \frac{R_{\mathrm{out}}^2}{\lambda^2}L_{\mathrm{out}}\right]^{-1}\sec^2(\theta)\left(\frac{\sigma_n}{\sigma_s}\right)^2, \end{aligned} \tag{4.34}$$

and

$$\begin{aligned} \mathrm{CRB}_{\mathrm{CUCA}}(\phi) &= F^{-1}_{\theta,\theta} \\ &= \frac{1}{4M\frac{\sigma_s^2}{\sigma_n^2}\left(R_{\mathrm{in}}^2 L_{\mathrm{in}} + R_{\mathrm{out}}^2 L_{\mathrm{out}}\right)\left(\frac{\pi}{\lambda}\sin(\theta)\right)^2} \\ &= \frac{1}{4\pi^2}\frac{1}{M}\frac{\lambda^2}{R_{\mathrm{in}}^2 L_{\mathrm{in}} + R_{\mathrm{out}}^2 L_{\mathrm{out}}}\left(\frac{\sigma_n}{\sigma_s}\right)^2 \csc^2(\theta) \\ &= \frac{1}{4\pi^2}\frac{1}{M}\left[\frac{R_{\mathrm{in}}^2}{\lambda^2}L_{\mathrm{in}} + \frac{R_{\mathrm{out}}^2}{\lambda^2}L_{\mathrm{out}}\right]^{-1}\csc^2(\theta)\left(\frac{\sigma_n}{\sigma_s}\right)^2. \end{aligned} \tag{4.35}$$

Consequently, the $\mathrm{CRB}(\theta)$ and the $\mathrm{CRB}(\phi)$ for the UCA can be given by

$$\begin{aligned}
\mathrm{CRB}_{\mathrm{UCA}}(\theta) &= \frac{1}{4M\frac{\sigma_s^2}{\sigma_n^2}R_{\mathrm{UCA}}^2 L_{\mathrm{UCA}}\left(\frac{\pi}{\lambda}\cos(\theta)\right)^2} \\
&= \frac{1}{4\pi^2}\frac{1}{M}\frac{\lambda^2}{R_{\mathrm{UCA}}^2 L_{\mathrm{UCA}}}\left(\frac{\sigma_n}{\sigma_s}\right)^2 \sec^2(\theta) \\
&= \frac{1}{4\pi^2}\frac{1}{M}\left[\frac{R_{\mathrm{UCA}}^2}{\lambda^2}L_{\mathrm{UCA}}\right]^{-1} \sec^2(\theta)\left(\frac{\sigma_n}{\sigma_s}\right)^2, \qquad (4.36)
\end{aligned}$$

and

$$\begin{aligned}
\mathrm{CRB}_{\mathrm{UCA}}(\phi) &= \frac{1}{4M\frac{\sigma_s^2}{\sigma_n^2}R_{\mathrm{UCA}}^2 L_{\mathrm{UCA}}\left(\frac{\pi}{\lambda}\sin(\theta)\right)^2} \\
&= \frac{1}{4\pi^2}\frac{1}{M}\frac{\lambda^2}{R_{\mathrm{UCA}}^2 L_{\mathrm{UCA}}}\left(\frac{\sigma_n}{\sigma_s}\right)^2 \csc^2(\theta) \\
&= \frac{1}{4\pi^2}\frac{1}{M}\left[\frac{R_{\mathrm{UCA}}^2}{\lambda^2}L_{\mathrm{UCA}}\right]^{-1} \csc^2(\theta)\left(\frac{\sigma_n}{\sigma_s}\right)^2. \qquad (4.37)
\end{aligned}$$

CHAPTER FIVE

DISCUSSION, CONCLUSION AND RECOMMENDATION

5.1 Discussion

Comparing the CUCA's CRBs in (4.34) - (4.35) and the UCA's CRBs in (4.36) - (4.37) it was found that the CRBs differed by the terms, $[R_{\text{in}}^2 L_{\text{in}} + R_{\text{out}}^2 L_{\text{out}}]^{-1}$ and $[R_{\text{UCA}}^2 L_{\text{UCA}}]^{-1}$. The interesting questions here were: What could be the smallest value of L_{UCA} such that the UCA and the CUCA have exactly equal performance? and what could be the corresponding value of R_{UCA}? Suppose there existed a constraint of $L_{\text{UCA}} = L_{\text{in}} + L_{\text{out}}$. Then, the smallest value of L_{UCA} was found such that the UCA and the CUCA performs equally and as a result, the corresponding value of R_{UCA} was computed. Now, it was supposed that $L_{\text{UCA}} = L_{\text{out}}$, then clearly, it implied that $L_{\text{in}} = 0$. Since for the UCA and the CUCA to perform the same, the equation $R_{\text{UCA}}^2 L_{\text{UCA}} = R_{\text{in}}^2 L_{\text{in}} + R_{\text{out}}^2 L_{\text{out}}$ holds, then the corresponding value of R_{UCA} was concluded to be given by,

$$R_{\text{UCA}} \;=\; +\sqrt{\frac{R_{\text{out}}^2 L_{\text{out}}}{L_{\text{UCA}}}}.$$

It was further noted that, the UCA and the CUCA had equal performance when the ratio of their CRBs was one and hence the below equation was found to hold,

$$R_{\text{UCA}}^2 L_{\text{UCA}} \;=\; \left(R_{\text{in}}^2 - R_{\text{out}}^2\right) L_{\text{in}} + R_{\text{out}}^2 L_{\text{UCA}},$$

which was also re-expressed as;

$$\left(R_{\text{UCA}}^2 - R^2\right) L_{\text{UCA}} \;=\; \left(R_{\text{in}}^2 - R_{\text{out}}^2\right) L_{\text{in}},$$

implying that,

$$\frac{L_{\text{in}}}{L_{\text{UCA}}} = \frac{R_{\text{UCA}}^2 - R_{\text{out}}^2}{R_{\text{in}}^2 - R_{\text{out}}^2}.$$

Therefore, the UCA and the CUCA were found to perform the same, if, $R_{\text{UCA}} = R_{\text{in}}$ and $L_{\text{UCA}} = L_{\text{in}}$ implying that $L_{\text{out}} = 0$ since $L_{\text{UCA}} = L_{\text{in}} + L_{\text{out}}$.
In addition, the CRBs would be smallest, if all sensors were to be placed on the outer circle (i.e. $L_{\text{in}} = 0$) and $R_{\text{UCA}} = R_{\text{out}} \to \infty$.

5.1.1 Special Cases

Special Case 1: If $R_{\text{in}} = (R_{\text{out}} - \frac{\lambda}{2})$

Equations (4.34) and (4.35) for the $\text{CRB}(\theta)$ and the $\text{CRB}(\phi)$ of the CUCA respectively became

$$\begin{aligned}
\text{CRB}_{\text{CUCA}}(\theta) &= \frac{1}{4M}\left(\frac{\lambda}{\pi}\right)^2 \frac{1}{\left(\left(R_{\text{out}} - \frac{\lambda}{2}\right)^2 L_{\text{in}} + R_{\text{out}}^2 L_{\text{out}}\right)} \left(\frac{\sigma_n}{\sigma_s}\right)^2 \sec^2(\theta) \\
&= \frac{1}{4\pi^2}\frac{1}{M}\frac{\lambda^2}{R_{\text{out}}^2\left(L_{\text{in}} + L_{\text{out}}\right) + \left(\frac{\lambda^2}{4} - R_{\text{out}}\lambda\right) L_{\text{in}}} \left(\frac{\sigma_n}{\sigma_s}\right)^2 \sec^2(\theta) \\
&= \frac{1}{4\pi^2}\frac{1}{M}\left(\frac{\sigma_n}{\sigma_s}\right)^2 \sec^2(\theta) \left[\frac{R_{\text{out}}^2}{\lambda^2}\left(L_{\text{in}} + L_{\text{out}}\right) + \left(\frac{1}{4} - \frac{R_{\text{out}}}{\lambda}\right) L_{\text{in}}\right]^{-1} \quad (5.1) \\
\text{CRB}_{\text{CUCA}}(\phi) &= \frac{1}{4M}\left(\frac{\lambda}{\pi}\right)^2 \frac{1}{\left(\left(R_{\text{out}} - \frac{\lambda}{2}\right)^2 L_{\text{in}} + R_{\text{out}}^2 L_{\text{out}}\right)} \left(\frac{\sigma_n}{\sigma_s}\right)^2 \csc^2(\theta) \\
&= \frac{1}{4\pi^2}\frac{1}{M}\frac{\lambda^2}{R_{\text{out}}^2\left(L_{\text{in}} + L_{\text{out}}\right) + \left(\frac{\lambda^2}{4} - R_{\text{out}}\lambda\right) L_{\text{in}}} \left(\frac{\sigma_n}{\sigma_s}\right)^2 \csc^2(\theta) \\
&= \frac{1}{4\pi^2}\frac{1}{M}\left(\frac{\sigma_n}{\sigma_s}\right)^2 \csc^2(\theta) \left[\frac{R_{\text{out}}^2}{\lambda^2}\left(L_{\text{in}} + L_{\text{out}}\right) + \left(\frac{1}{4} - \frac{R_{\text{out}}}{\lambda}\right) L_{\text{in}}\right]^{-1} \quad (5.2)
\end{aligned}$$

by expansion of the term, $(R_{\text{out}} - \frac{\lambda}{2})^2$ and putting like terms together.

Special Case 2: If furthermore $L_{\text{in}} = 4$ and $L_{\text{out}} = L_{\text{UCA}} - 4$

Equations (5.1) and (5.2) became

$$\begin{aligned}
\text{CRB}_{\text{CUCA}}(\theta) &= \frac{1}{4M}\left(\frac{\lambda}{\pi}\right)^2 \frac{1}{\left(\left(R_{\text{out}}^2 - \frac{\lambda}{2}\right)^2 4 + R_{\text{out}}^2(L_{\text{UCA}} - 4)\right)} \left(\frac{\sigma_n}{\sigma_s}\right)^2 \sec^2(\theta) \\
&= \frac{1}{4\pi^2}\frac{1}{M}\frac{\lambda^2 \sec^2(\theta)}{R_{\text{out}}^2 L_{\text{UCA}} - 4R_{\text{out}}\lambda + \lambda^2}\left(\frac{\sigma_n}{\sigma_s}\right)^2 \\
&= \frac{1}{4\pi^2}\frac{1}{M}\left[\frac{R_{\text{out}}^2}{\lambda^2}L_{\text{UCA}} - 4\frac{R_{\text{out}}}{\lambda} + 1\right]^{-1} \sec^2(\theta)\left(\frac{\sigma_n}{\sigma_s}\right)^2, \qquad (5.3) \\
\text{CRB}_{\text{CUCA}}(\phi) &= \frac{1}{4M}\left(\frac{\lambda}{\pi}\right)^2 \frac{1}{\left(\left(R_{\text{out}}^2 - \frac{\lambda}{2}\right)^2 4 + R_{\text{out}}^2(L_{\text{UCA}} - 4)\right)} \left(\frac{\sigma_n}{\sigma_s}\right)^2 \csc^2(\theta) \\
&= \frac{1}{4\pi^2}\frac{1}{M}\frac{\lambda^2 \csc^2(\theta)}{R_{\text{out}}^2 L_{\text{UCA}} - 4R_{\text{out}}\lambda + \lambda^2}\left(\frac{\sigma_n}{\sigma_s}\right)^2 \\
&= \frac{1}{4\pi^2}\frac{1}{M}\left[\frac{R_{\text{out}}^2}{\lambda^2}L_{\text{UCA}} - 4\frac{R_{\text{out}}}{\lambda} + 1\right]^{-1} \csc^2(\theta)\left(\frac{\sigma_n}{\sigma_s}\right)^2. \qquad (5.4)
\end{aligned}$$

5.1.2 The Proposed Geometry

Imposed on the aforementioned 2-circle concentric and uniform array geometry were these additional constraints:

(i) $R_{\text{out}} = R_{\text{in}} + \frac{\lambda}{2}$.

(ii) L_{out} is wholly divisible by 4.

(iii) $L_{\text{in}} = 4$. Constraints (ii)-(iii) together produce four pairs of half-wavelength-spaced sensors, with one pair each along the positive x-axis, the negative x-axis, the positive y-axis, and the negative y-axis as shown in figure 5.1.

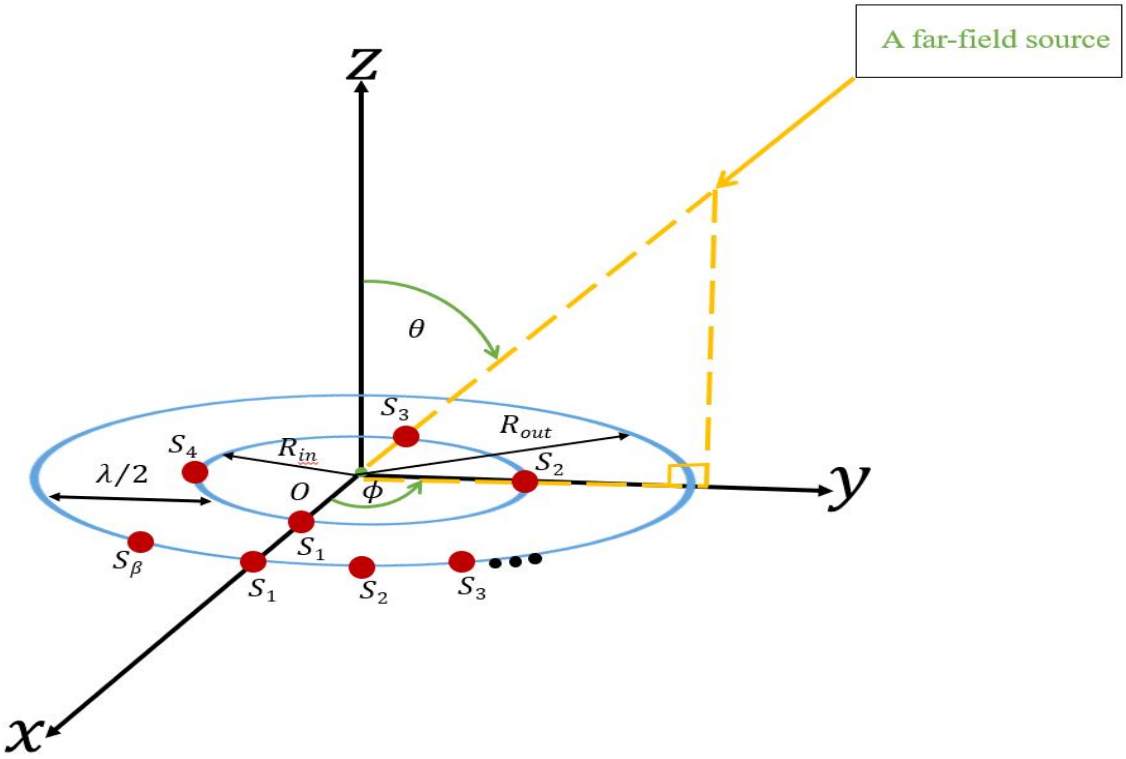

Figure 5.1: The Proposed Geometry. β denotes $L_{\mathrm{UCA}} - 4$.

The above ensures (a) half-wavelength spacing along each of the two Cartesian dimensions of the present planar array grid, (b) circular symmetry about the Cartesian origin, (c) a maximum number of sensors on the outer circle.

Using the above constraints, equations (5.1) – (5.2) or (5.3) – (5.4) gave

$$\begin{aligned} & (2\pi)^2 M \left(\frac{\sigma_s}{\sigma_n}\right)^2 \cos^2(\theta)\mathrm{CRB}_{\mathrm{CUCA}}(\theta) \\ = & \left[(L_{\mathrm{out}}+4)\left(\frac{R_{\mathrm{out}}}{\lambda}\right)^2 - 4\frac{R_{\mathrm{out}}}{\lambda} + 1\right]^{-1} := \tilde{\mathrm{CRB}} \\ \equiv & (2\pi)^2 M \left(\frac{\sigma_s}{\sigma_n}\right)^2 \sin^2(\theta)\mathrm{CRB}_{\mathrm{CUCA}}(\phi). \end{aligned} \tag{5.5}$$

Since $R_{\mathrm{in}} \geq 0$, then from constraint (i), $R_{\mathrm{out}} \geq \frac{\lambda}{2}$ which implied that $\frac{R_{\mathrm{out}}}{\lambda} \geq \frac{1}{2}$.

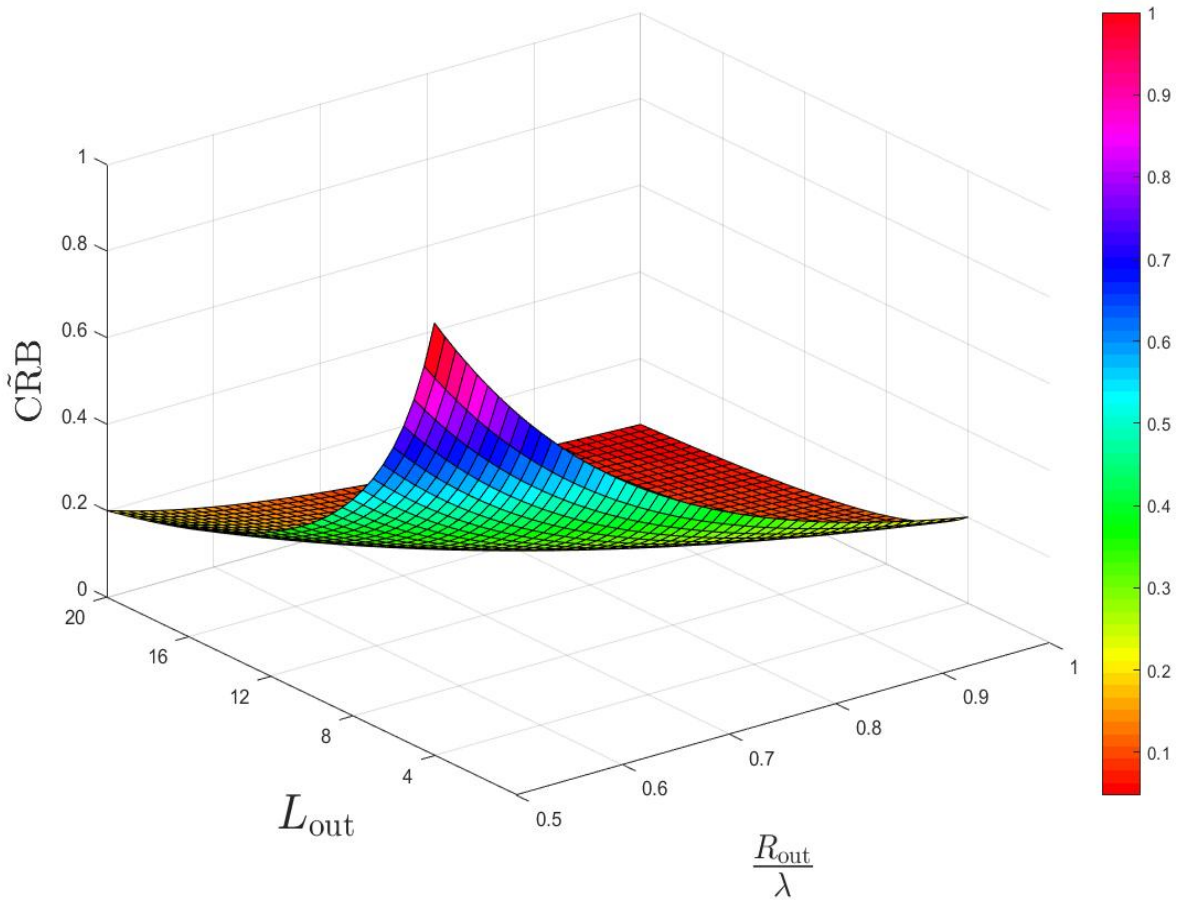

Figure 5.2: Variation of the CRBs with respect to $\frac{R_{\text{out}}}{\lambda}$ and L_{out}. Refer to equation (5.5).

From Figure 5.2, it is clear that the CRBs decrease with increase in L_{out} and/or $\frac{R_{\text{out}}}{\lambda}$, which is expected. Analytical explanation to this observation is given below.

From the graph above, the turning point with respect to R_{out} using (5.5) is given by

$$\begin{aligned}\frac{\partial \text{C}\tilde{\text{R}}\text{B}}{\partial R_{\text{out}}} &= \frac{-2(L_{\text{out}}+4)\frac{R_{\text{out}}}{\lambda}+4}{\left((L_{\text{out}}+4)\left(\frac{R_{\text{out}}}{\lambda}\right)^2-4\frac{R_{\text{out}}}{\lambda}+1\right)^2} \\ &= 0,\end{aligned}$$

which implies that the turning point occurs when

$$\frac{R_{\text{out}}}{\lambda} = \frac{2}{L_{\text{out}}+4}.$$

However, since $L_{\text{out}} > 0$, then $\frac{R_{\text{out}}}{\lambda} \leq 0.5$ which is the minimum point of $\frac{R_{\text{out}}}{\lambda}$ in Figure 5.2. Hence the graph has no turning point with respect to $\frac{R_{\text{out}}}{\lambda}$ and thus $\text{C}\tilde{\text{R}}\text{B}$ decreases with increase in $\frac{R_{\text{out}}}{\lambda}$. This observation is also clear from (5.5) since the numerator is a

constant, and the denominator $L_{\text{out}}\left(\frac{R_{\text{out}}}{\lambda}\right)^2 + 4\left(\frac{R_{\text{out}}}{\lambda}\right)^2 - 4\frac{R_{\text{out}}}{\lambda} + 1 \gg 1$ as $\frac{R_{\text{out}}}{\lambda}$ increases.

Similarly, the turning point with respect to L_{out} was given by

$$\begin{aligned}\frac{\partial \tilde{\text{CRB}}}{\partial L_{\text{out}}} &= \frac{-\left(\frac{R_{\text{out}}}{\lambda}\right)^2}{\left((L_{\text{out}}+4)\left(\frac{R_{\text{out}}}{\lambda}\right)^2 - 4\frac{R_{\text{out}}}{\lambda} + 1\right)^2} \\ &= 0,\end{aligned}$$

which implied that the turning point occurs when

$$\frac{R_{\text{out}}}{\lambda} = 0$$

which is infeasible since $\frac{R_{\text{out}}}{\lambda} \geq 0.5$. Hence the graph has no turning point with respect to L_{out} and thus $\tilde{\text{CRB}}$ decreases with increase in L_{out}. This observation was also clear from (5.5) since the numerator is a constant, and the denominator $L_{\text{out}}\left(\frac{R_{\text{out}}}{\lambda}\right)^2 + 4\left(\frac{R_{\text{out}}}{\lambda}\right)^2 - 4\frac{R_{\text{out}}}{\lambda} + 1 \gg 1$ as L_{out} increases.

5.1.3 A Single-Circle

For a single-circle with $\frac{\lambda}{2}$ inter-sensor spacing with L_{tot} number of sensors we had

$$L_{\text{tot}} \;=\; \frac{\pi}{\sin^{-1}\left(\frac{\lambda}{4R_{\text{UCA}}}\right)}.$$

Using equations $(4.36) - (4.37)$ we obtain,

$$\begin{aligned}(2\pi)^2 M\left(\frac{\sigma_s}{\sigma_n}\right)^2 \cos^2(\theta)\text{CRB}(\theta) \;&=\; \left[\left(\frac{R_{\text{UCA}}}{\lambda}\right)^2 L_{\text{tot}}\right]^{-1} \;:=\; \tilde{\text{CRB}}_{\text{UCA},\frac{\lambda}{2}} \quad (5.6)\\ &\equiv\; (2\pi)^2 M\left(\frac{\sigma_s}{\sigma_n}\right)^2 \sin^2(\theta)\text{CRB}(\phi).\end{aligned}$$

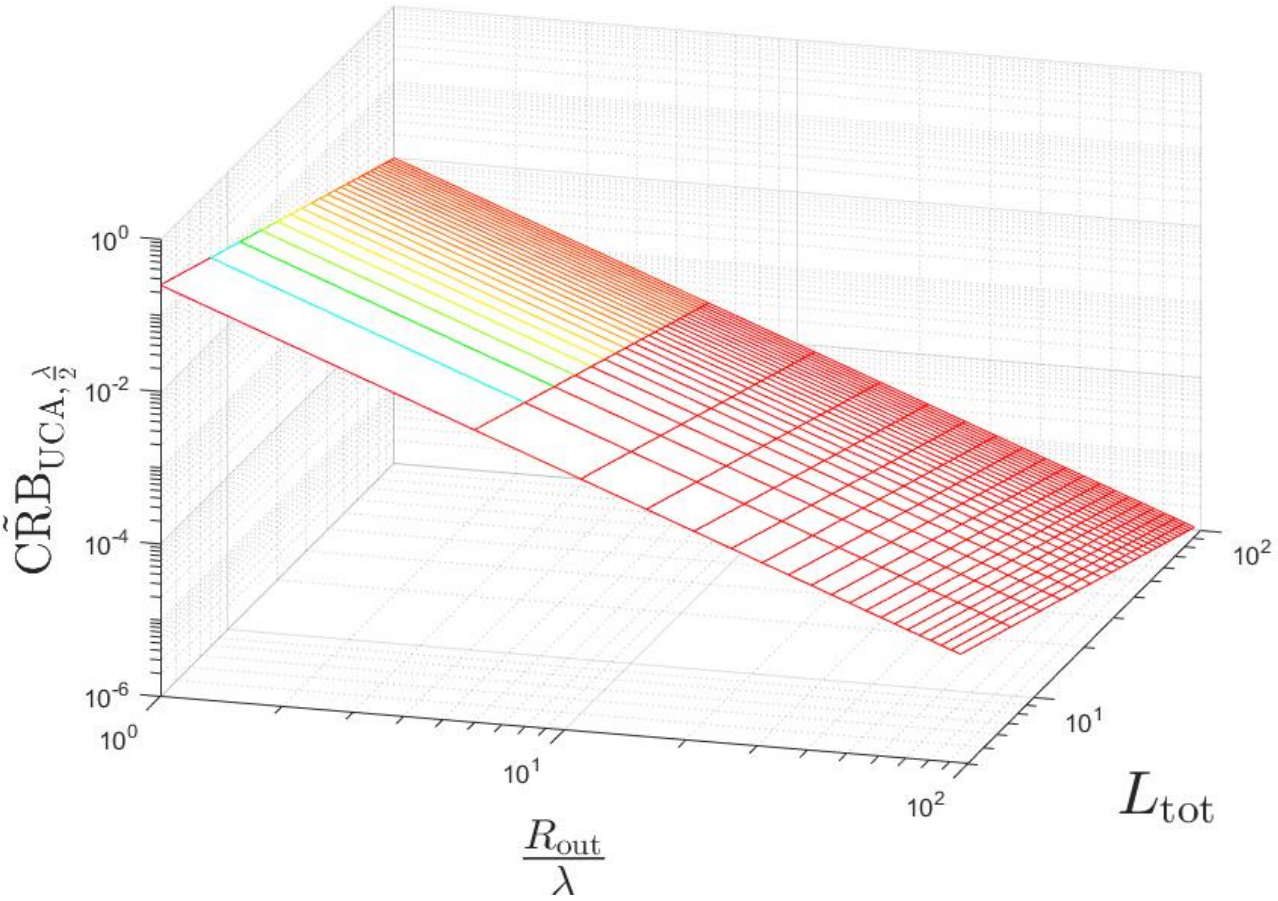

Figure 5.3: Variation of the UCA's CRB with the total number of sensors (L_{tot}) and the wavelength-normalized radius ($\frac{R_{\text{out}}}{\lambda} = \frac{R_{\text{UCA}}}{\lambda}$). Refer to equation (5.6).

5.1.4 A 2-Circle Array with Equal Number of Sensors in Each Circle

The 2-circle array geometry had the following properties

a) each circle had $\frac{L_{tot}}{2}$ number of sensors,

b) the 2-circles radii differed by $\frac{\lambda}{2}$ (i.e $R_{\text{out}} = R_{\text{in}} + \frac{\lambda}{2}$), and

c) each sensor on the outer circle was matched with one sensor on the inner circle.

Using the above information and equations (4.34) − (4.35) yields

$$\begin{aligned}(2\pi)^2 M \left(\frac{\sigma_s}{\sigma_n}\right)^2 \cos^2(\theta)\text{CRB}(\theta) &= \frac{1}{2\left(\frac{R_{\text{in}}}{\lambda}\right)^2 + \frac{R_{\text{in}}}{\lambda} + \frac{1}{4}} \frac{2}{L_{\text{tot}}} := \tilde{\text{CRB}}_{L_{\text{in}}=L_{\text{out}}} \quad (5.7)\\ &\equiv (2\pi)^2 M \left(\frac{\sigma_s}{\sigma_n}\right)^2 \sin^2(\theta)\text{CRB}(\phi).\end{aligned}$$

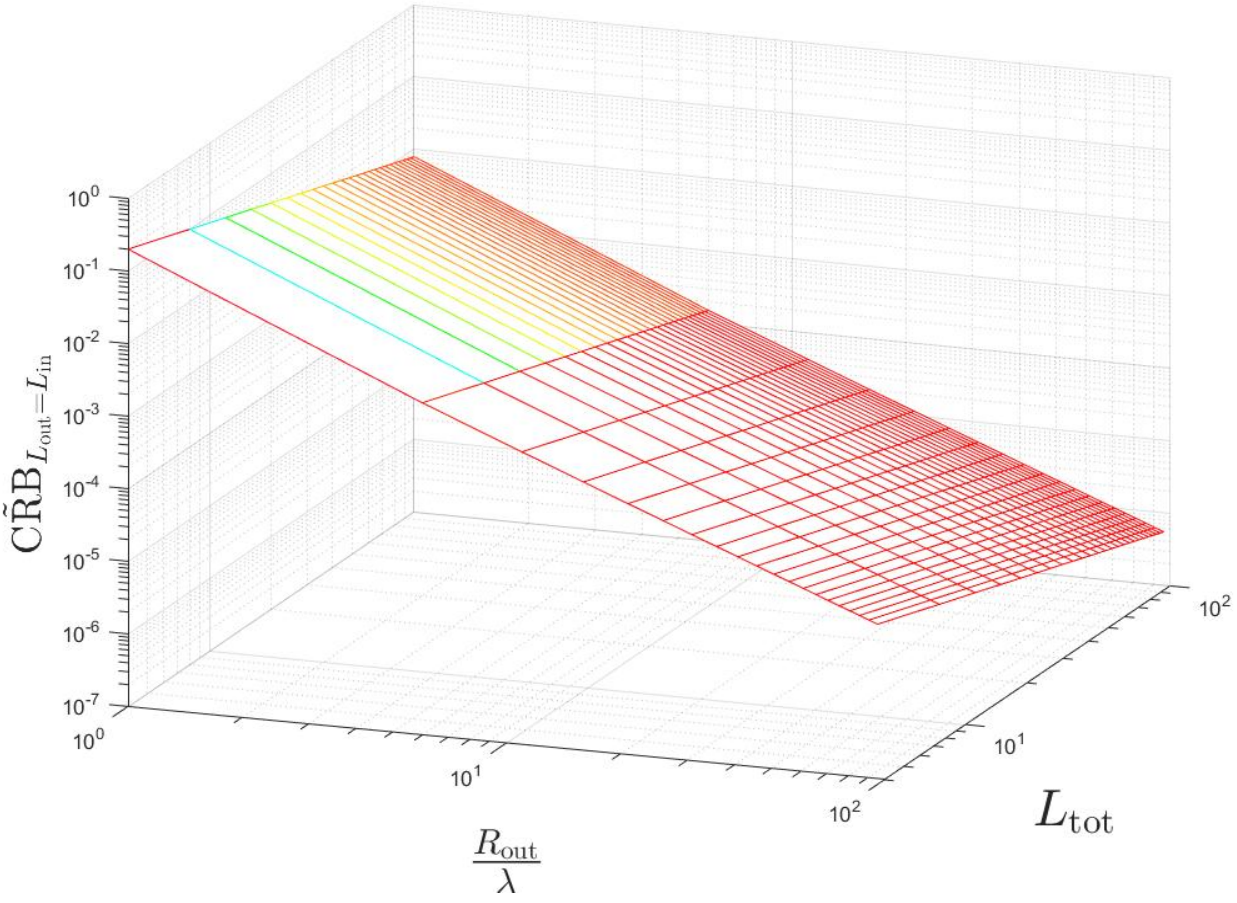

Figure 5.4: Variation of the 2-circle array's (with equal number of sensors in each circle) CRB with the total number of sensors (L_{tot}) and the wavelength-normalized radius ($\frac{R_{\text{out}}}{\lambda}$). Refer to equation (5.7).

Estimation Accuracy's Comparative Graph for the Proposed geometry, A Single Circle, and a 2-Circle Array (with equal ($\frac{L_{\text{tot}}}{2}$) number of sensors in each circle) All with Equal (L_{tot}) Number of sensors

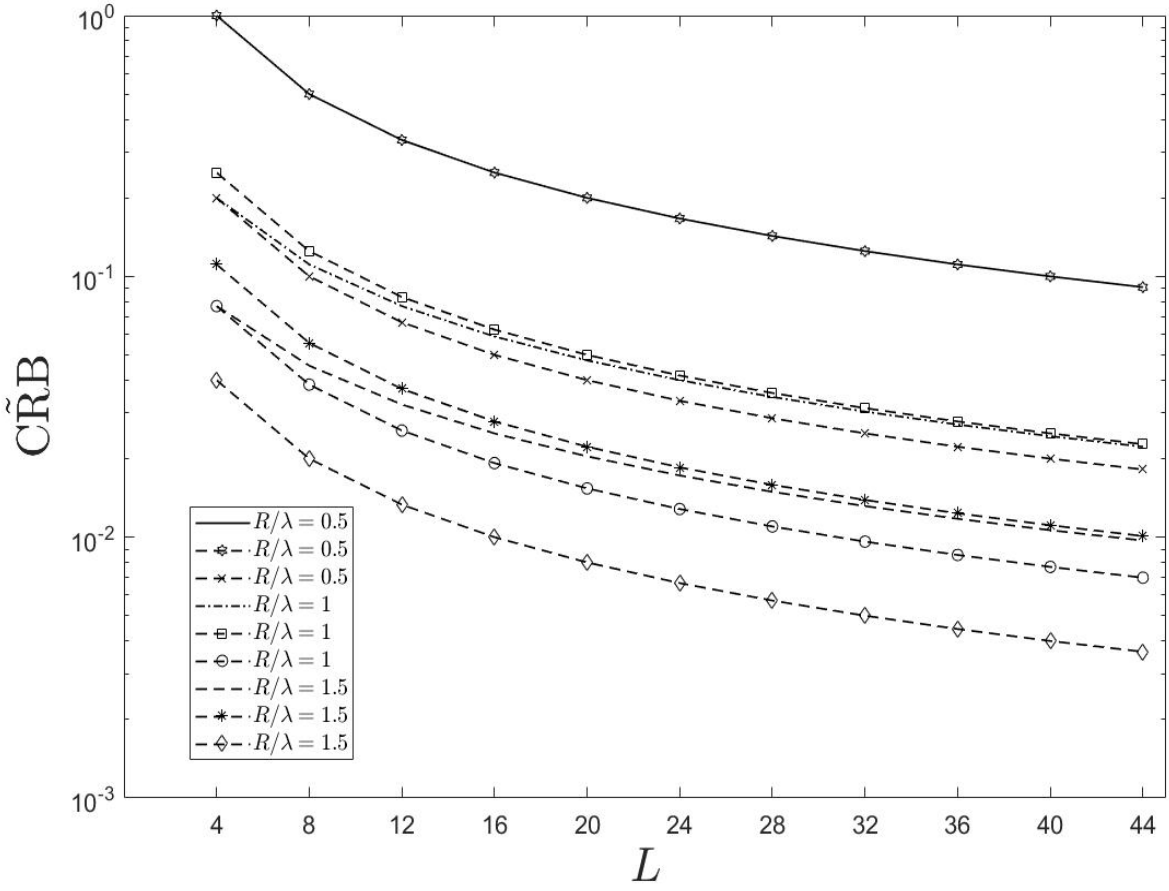

Figure 5.5: CRBs variations of the Proposed geometry, a single circle, and a 2-circle array (with equal ($\frac{L_{\text{tot}}}{2}$) number of sensors in each circle) with the total number of sensors ($L_{\text{tot}} = L$) at different values of the wavelength-normalized radius ($\frac{R}{\lambda}$) (5.5), (5.6) and (5.7)

From Figure 5.5, it was generally deduced that, the CRBs for all the three geometries decrease gently with increase in the number of sensors (L) at different values of $\frac{R}{\lambda}$. However, the 2-circle geometry (the solid, the dashed-dot and the dashed curves) and the single-circle geometry (the dashed-hexagon, the dashed-square, and dashed-asterisks curves) have exactly equal performance at $\frac{R}{\lambda} = 0 \cdot 5$ but thereafter, the 2-circle geometry has lower CRB for all $\frac{R}{\lambda} > 0 \cdot 5$.

Importantly, of all the three geometries, the proposed geometry (the dashed-cross, the dashed-circle and the dashed-diamond curves) has the lowest CRBs for all values of $\frac{R}{\lambda}$. Furthermore, in all the geometries, increase in $\frac{R}{\lambda}$ reduces the CRBs. This is possibly due to increased aperture.

5.1.5 Numerical Case

As aforementioned, the CUCA's and the UCA's CRBs in (4.34) - (4.35) and (4.36) - (4.37) respectively differed by the terms, $[R_{\mathrm{in}}^2 L_{\mathrm{in}} + R_{\mathrm{out}}^2 L_{\mathrm{out}}]^{-1}$ and $[R_{\mathrm{UCA}}^2 L_{\mathrm{UCA}}]^{-1}$. Now, with the array's aperture enlargement strategy, $R_{\mathrm{out}} >> R_{\mathrm{UCA}}$ implying that $R_{\mathrm{in}} + R_{\mathrm{out}} >> R_{\mathrm{UCA}}$. Also $R_{\mathrm{in}} L_{\mathrm{in}} + R_{\mathrm{out}} L_{\mathrm{out}} > R_{\mathrm{UCA}} L_{\mathrm{UCA}}$ since $L_{\mathrm{UCA}} = L_{\mathrm{in}} + L_{\mathrm{out}}$ which implied that $[R_{\mathrm{in}}^2 L_{\mathrm{in}} + R_{\mathrm{out}}^2 L_{\mathrm{out}}]^{-1} < [R_{\mathrm{UCA}}^2 L_{\mathrm{UCA}}]^{-1}$. For example, an arbitrary choice was made that, $R_{\mathrm{out}} = 20$ units, $R_{\mathrm{in}} = 8$ units, $R_{\mathrm{UCA}} = 12$ units, $L_{\mathrm{UCA}} = 12$, $L_{\mathrm{out}} = 8$ and $L_{\mathrm{in}} = 4$. Substituting these values in $[R_{\mathrm{in}}^2 L_{\mathrm{in}} + R_{\mathrm{out}}^2 L_{\mathrm{out}}]^{-1}$ and $[R_{\mathrm{UCA}}^2 L_{\mathrm{UCA}}]^{-1}$ respectively, then it was found that $[R_{\mathrm{in}}^2 L_{\mathrm{in}} + R_{\mathrm{out}}^2 L_{\mathrm{out}}]^{-1} = \frac{1}{3456}$ and $[R_{\mathrm{UCA}}^2 L_{\mathrm{UCA}}]^{-1} = \frac{1}{1728}$ which clearly implied that $[R_{\mathrm{in}}^2 L_{\mathrm{in}} + R_{\mathrm{out}}^2 L_{\mathrm{out}}]^{-1} < [R_{\mathrm{UCA}}^2 L_{\mathrm{UCA}}]^{-1}$. This numerical example and any other example satisfying the above conditions would further verify that the 2-circle concentric uniform array has lower CRB than the single ring array and therefore has better performance.

5.1.6 Further Comparison in Estimation Accuracy of Three Versions of the 2-Circle Concentric Uniform Array

These 3-versions were equal in size since they were derived from a single 2-ring concentric array and had equal number of sensors (i.e define $L_{\text{sum}} = L_{\text{inner}} + L_{\text{outer}}$) but with different distributions in each ring. The two rings in each version differed by $\frac{\lambda}{4}$ such that $R_{\text{outer}} = R_{\text{inner}} + \frac{\lambda}{4}$ or $R_{\text{inner}} = R_{\text{outer}} - \frac{\lambda}{4}$.

Version One

This version had slightly greater number of sensors on the outer ring than the inner ring i.e

(i) $L_{\text{inner}} = 8$

(ii) $L_{\text{outer}} = L_{\text{sum}} - 8$

(iii) $R_{\text{inner}} = R_{\text{outer}} - \frac{\lambda}{4}$

(iv) at least 4 sensors on the inner ring lie on positive and negative x-y intercepts.

For the above properties, see the illustration on Figure 5.6.

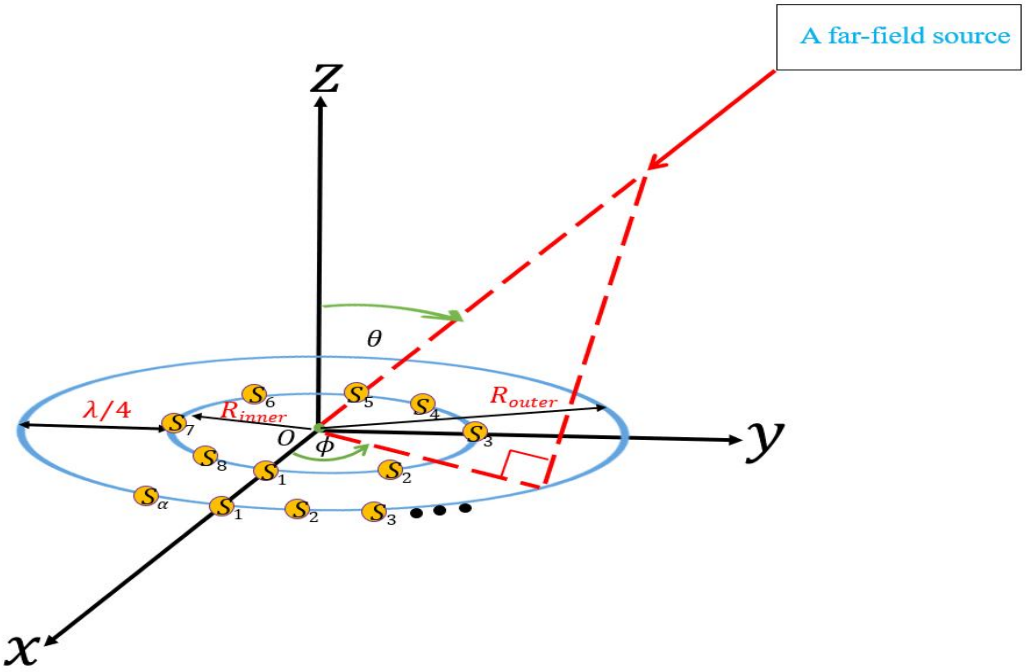

Figure 5.6: Version one of the 2-ring concentric planar array with slightly greater number of isotropic sensors on the outer ring than the inner ring. α represents $L_{\text{sum}} - 8$.

Using the constraints (i)-(iii) in (4.34)-(4.35), the CRBs for version one were given by

$$\mathrm{CRB}_{\mathrm{V}_1}(\theta) = \frac{1}{4\pi^2}\frac{1}{M}\left(\frac{\sigma_n}{\sigma_s}\right)^2 \sec^2(\theta)\left[\left(\frac{R_{\mathrm{outer}}}{\lambda}\right)^2 L_{\mathrm{sum}} - 4\frac{R_{\mathrm{outer}}}{\lambda} + \frac{1}{2}\right]^{-1}, \quad (5.8)$$

$$\mathrm{CRB}_{\mathrm{V}_1}(\phi) = \frac{1}{4\pi^2}\frac{1}{M}\left(\frac{\sigma_n}{\sigma_s}\right)^2 \csc^2(\theta)\left[\left(\frac{R_{\mathrm{outer}}}{\lambda}\right)^2 L_{\mathrm{sum}} - 4\frac{R_{\mathrm{outer}}}{\lambda} + \frac{1}{2}\right]^{-1}. \quad (5.9)$$

Version One's Graph

Equating (5.8) to (5.9) we had

$$\begin{aligned} & (2\pi)^2 M\left(\frac{\sigma_s}{\sigma_n}\right)^2 \cos^2(\theta)\mathrm{CRB}_{\mathrm{V}_1}(\theta) \\ = & \left[\left(\frac{R_{\mathrm{outer}}}{\lambda}\right)^2 L_{\mathrm{sum}} - 4\frac{R_{\mathrm{outer}}}{\lambda} + \frac{1}{2}\right]^{-1} := \widetilde{\mathrm{CRB}}_{\mathrm{V}_1} \quad (5.10) \\ = & (2\pi)^2 M\left(\frac{\sigma_s}{\sigma_n}\right)^2 \sin^2(\theta)\mathrm{CRB}_{\mathrm{V}_1}(\phi). \end{aligned}$$

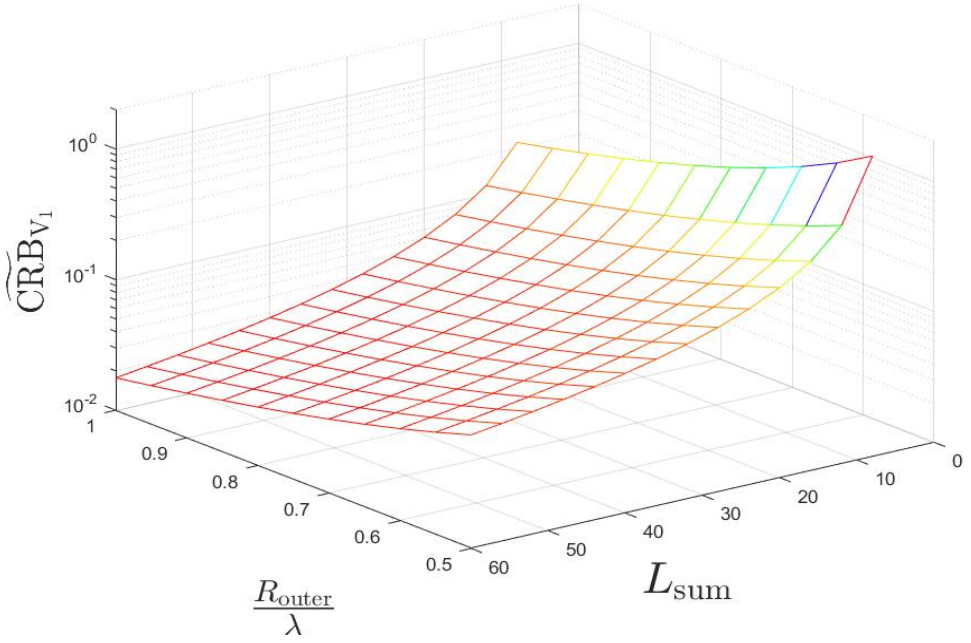

Figure 5.7: Variation of version one's CRB with the total number of sensors (L_{sum}) and the wavelength-normalized radius ($\frac{R_{\mathrm{outer}}}{\lambda}$). Refer to equation (5.10).

Observations From Figure 5.7

1. The $\widetilde{\mathrm{CRB}}_{\mathrm{V}_1}$ decreases gently with increase in L_{sum} (total number of sensors),

2. The $\widetilde{\mathrm{CRB}}_{\mathrm{V}_1}$ decreases gently with increase in $\frac{R_{\mathrm{outer}}}{\lambda}$ (wavelength-normalized radius).

Version Two

This version had equal number of sensors on each ring i.e

1. $R_{\mathrm{inner}} = R_{\mathrm{outer}} - \frac{\lambda}{4}$,

2. each ring had $\frac{L_{\mathrm{sum}}}{2}$ number of sensors,

3. the sensors on the inner ring and the sensors on the outer ring were matched at the same azimuth angle.

The above properties are displayed in Figure 5.8.

Using the properties (1)-(2) in (4.34)-(4.35), the CRBs for version two were found to be

$$\mathrm{CRB}_{\mathrm{V}_2}(\theta) = \frac{1}{4\pi^2}\frac{1}{M}\left(\frac{\sigma_n}{\sigma_s}\right)^2 \sec^2(\theta)\left[2\left(\frac{R_{\mathrm{outer}}}{\lambda}\right)^2 - \frac{R_{\mathrm{outer}}}{2\lambda} + \frac{1}{16}\right]^{-1}\frac{2}{L_{\mathrm{sum}}} \quad (5.11)$$

$$\mathrm{CRB}_{\mathrm{V}_2}(\phi) = \frac{1}{4\pi^2}\frac{1}{M}\left(\frac{\sigma_n}{\sigma_s}\right)^2 \csc^2(\theta)\left[2\left(\frac{R_{\mathrm{outer}}}{\lambda}\right)^2 - \frac{R_{\mathrm{outer}}}{2\lambda} + \frac{1}{16}\right]^{-1}\frac{2}{L_{\mathrm{sum}}} \quad (5.12)$$

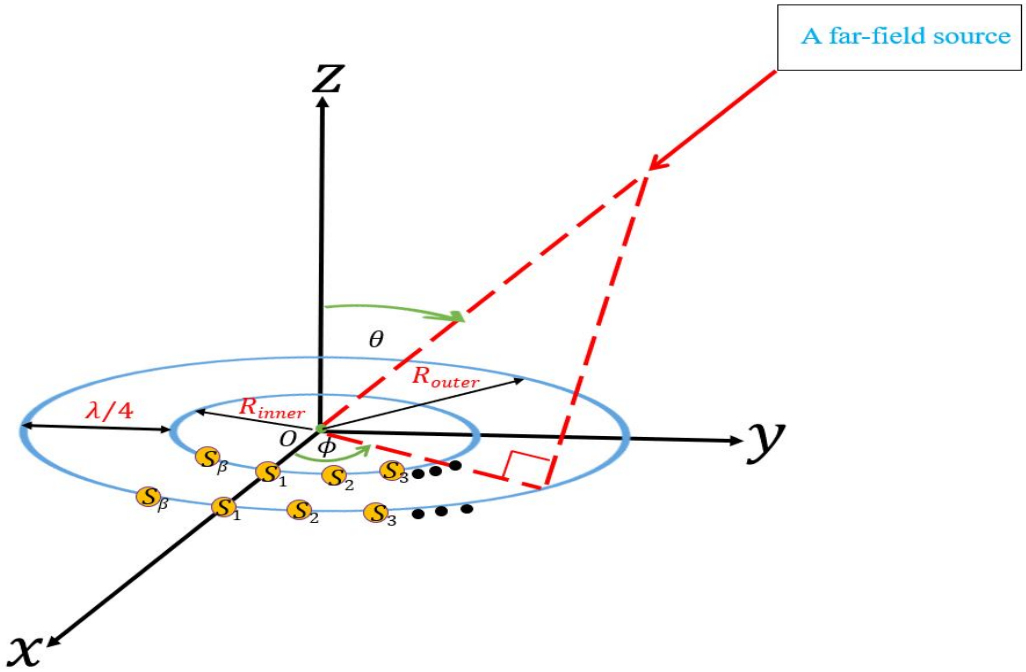

Figure 5.8: Version two of the 2-ring concentric planar array with equal number of isotropic sensors on both the outer ring and the inner ring. β symbolizes $L_{\text{inner}} = L_{\text{outer}} = \frac{L_{\text{sum}}}{2}$.

Version Two's Graph

Equating (5.11) to (5.12) we obtain,

$$\begin{aligned} & (2\pi)^2 M \left(\frac{\sigma_s}{\sigma_n}\right)^2 \cos^2(\theta)\text{CRB}_{\text{V}_2}(\theta) \\ = \; & \frac{2}{L_{\text{sum}}}\left[2\left(\frac{R_{\text{outer}}}{\lambda}\right)^2 - \frac{R_{\text{outer}}}{2\lambda} + \frac{1}{16}\right]^{-1} := \widetilde{\text{CRB}}_{\text{V}_2} \qquad (5.13) \\ = \; & (2\pi)^2 M \left(\frac{\sigma_s}{\sigma_n}\right)^2 \sin^2(\theta)\text{CRB}_{\text{V}_2}(\phi). \end{aligned}$$

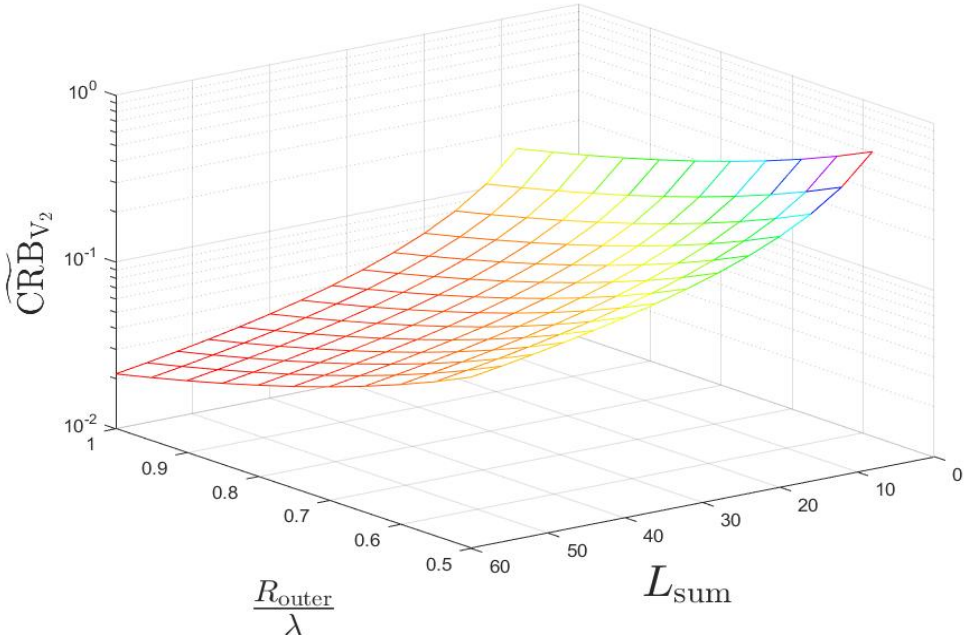

Figure 5.9: Variation of version's two's CRB with the total number of sensors (L_{sum}) and the wavelength-normalized radius ($\frac{R_{\mathrm{outer}}}{\lambda}$). Refer to equation (5.13).

Observations From Figure 5.9

1. The $\widetilde{\mathrm{CRB}}_{\mathrm{V}_2}$ decreases gently with increase in L_{sum} (total number of sensors),

2. The $\widetilde{\mathrm{CRB}}_{\mathrm{V}_2}$ decreases gently with increase in $\frac{R_{\mathrm{outer}}}{\lambda}$ (wavelength-normalized radius).

Version Three

This version had slightly greater number of sensors on the inner ring than the outer ring i.e

(i) $L_{\mathrm{outer}} = 8$

(ii) $L_{\mathrm{inner}} = L_{\mathrm{sum}} - 8$

(iii) $R_{\mathrm{inner}} = R_{\mathrm{outer}} - \frac{\lambda}{4}$

(iv) Atleast 4 sensors on the outer ring lie on positive and negative x-y intercepts.

For the above properties, see the the illustration on Figure 5.10.

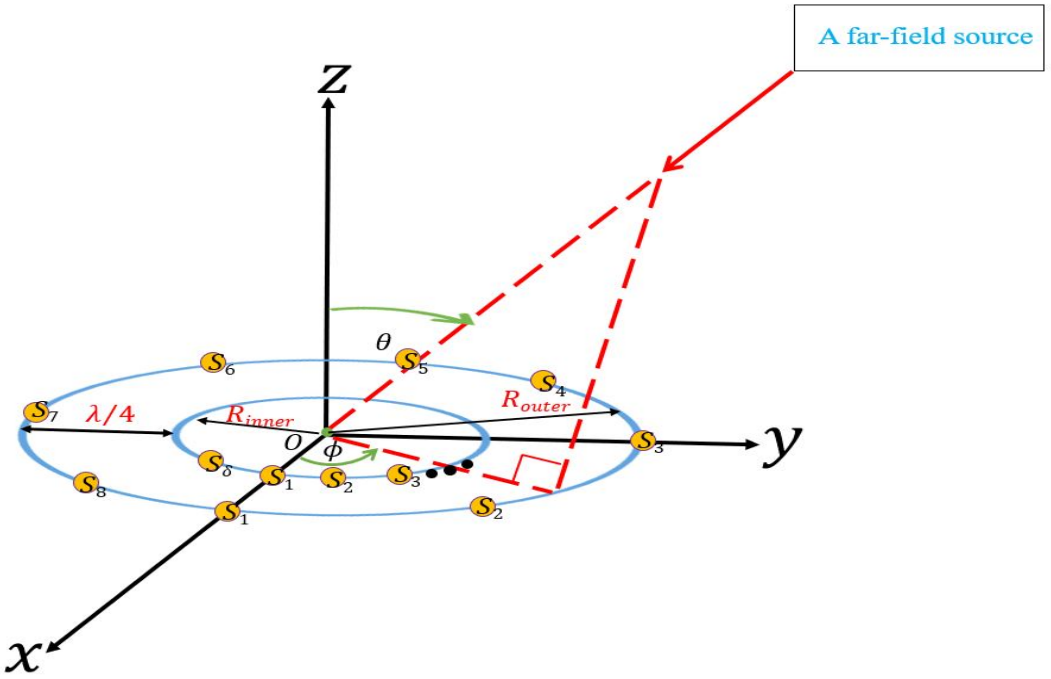

Figure 5.10: Version three of the 2-ring concentric planar array with slightly greater number of isotropic sensors on the inner ring than the outer ring. δ represents $L_{\text{sum}} - 8$.

Using the properties (i)-(iii) in (4.34)-(4.35), the CRBs for version three were found to be

$$\text{CRB}_{\text{V}_3}(\theta) = \frac{1}{4\pi^2}\frac{1}{M}\left(\frac{\sigma_n}{\sigma_s}\right)^2 \sec^2(\theta)\left[\left(\left(\frac{R_{\text{outer}}}{\lambda}\right)^2 - \frac{R_{\text{outer}}}{2\lambda} + \frac{1}{16}\right)L_{\text{sum}} + 4\frac{R_{\text{outer}}}{\lambda} - \frac{1}{2}\right]^{-1} \quad (5.14)$$

$$\text{CRB}_{\text{V}_3}(\phi) = \frac{1}{4\pi^2}\frac{1}{M}\left(\frac{\sigma_n}{\sigma_s}\right)^2 \csc^2(\theta)\left[\left(\left(\frac{R_{\text{outer}}}{\lambda}\right)^2 - \frac{R_{\text{outer}}}{2\lambda} + \frac{1}{16}\right)L_{\text{sum}} + 4\frac{R_{\text{outer}}}{\lambda} - \frac{1}{2}\right]^{-1} \quad (5.15)$$

Version Three's graph

Equating (5.14) to (5.15) we had

$$\begin{aligned}
&(2\pi)^2 M\left(\frac{\sigma_s}{\sigma_n}\right)^2 \cos^2(\theta)\text{CRB}_{\text{V}_3}(\theta) \\
= &\left[\left(\left(\frac{R_{\text{outer}}}{\lambda}\right)^2 - \frac{R_{\text{outer}}}{2\lambda} + \frac{1}{16}\right)L_{\text{sum}} + 4\frac{R_{\text{outer}}}{\lambda} - \frac{1}{2}\right]^{-1} := \widetilde{\text{CRB}}_{\text{V}_3} \\
= &\ (2\pi)^2 M\left(\frac{\sigma_s}{\sigma_n}\right)^2 \sin^2(\theta)\text{CRB}_{\text{V}_3}(\phi). \qquad (5.16)
\end{aligned}$$

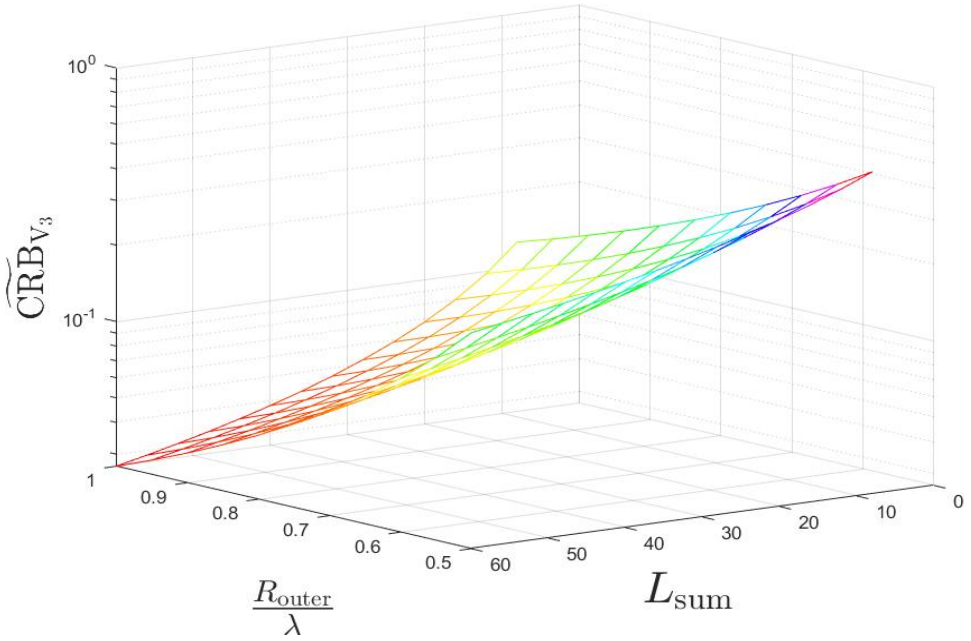

Figure 5.11: Variation of version three's CRB with the total number of sensors (L_{sum}) and the wavelength-normalized radius ($\frac{R_{\mathrm{outer}}}{\lambda}$). Refer to equation (5.16).

Observations From Figure 5.11

1. The $\widetilde{\mathrm{CRB}}_{\mathrm{V}_3}$ decreases sharp-gently with increase in L_{sum} (total number of sensors),

2. The $\widetilde{\mathrm{CRB}}_{\mathrm{V}_3}$ decreases sharp-gently with increase in $\frac{R_{\mathrm{outer}}}{\lambda}$ (wavelength-normalized radius).

Estimation Accuracy's Comparative Graph for the Three Versions of the 2-Circle Concentric Uniform Array Using Equations (5.10)-(5.16)

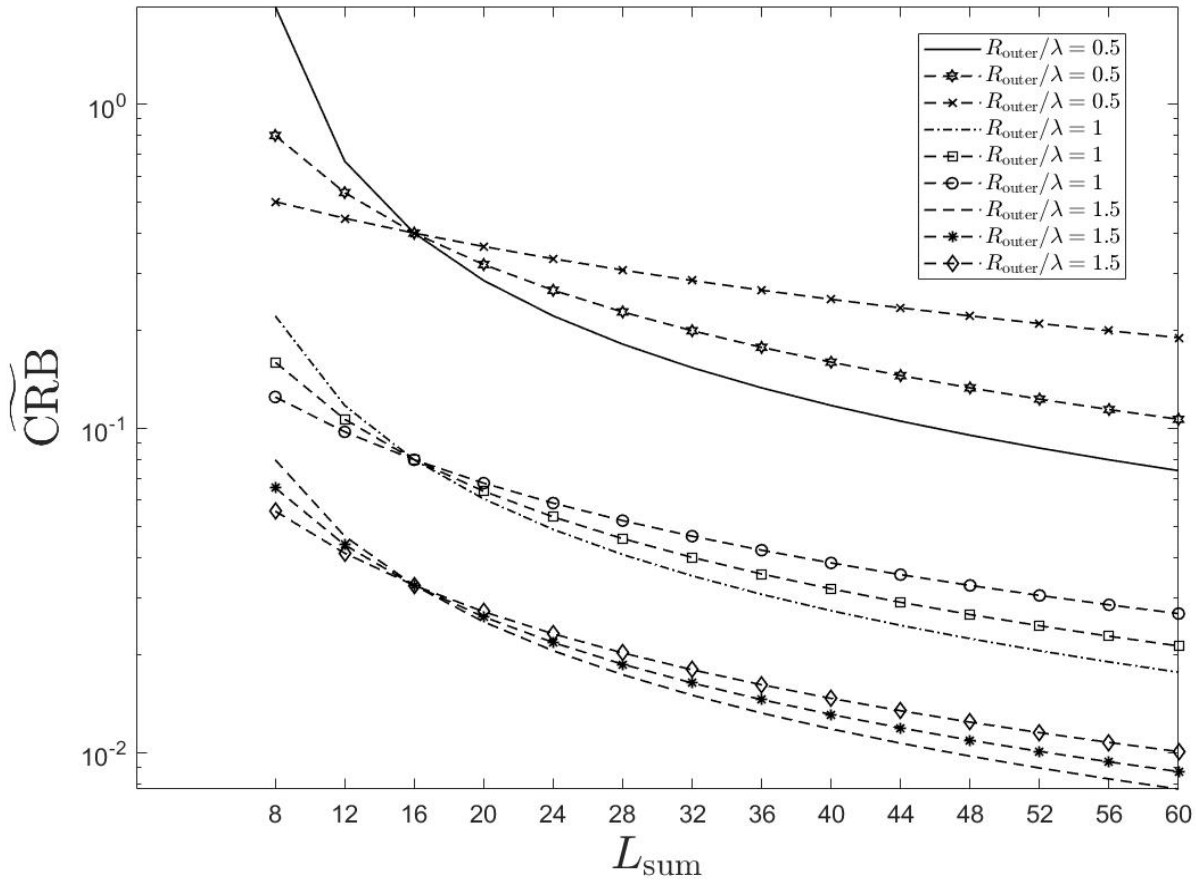

Figure 5.12: Comparison of the variation of the 3-versions' CRBs with the total number of sensors at different values of $\frac{R_{\text{outer}}}{\lambda}$. Refer to equations (5.10)-(5.16).

Version 1: Represented by the solid, the dashed-dot and the dashed curves, for different values of R_{out}/λ. Refer to equation (5.10).

Version 2: Represented by the dashed-hexagon, the dashed-square and the dashed-star curves, for different values of R_{out}/λ. Refer to equation (5.13).

Version 3: Represented by dash-cross, the dashed-circle and the dashed-diamond curves, for different values of R_{out}/λ. Refer to equation (5.16).

Observations From Figure 5.12

1. Generally, the CRBs decrease with increase in the number of sensors at all values of $\frac{R_{\mathrm{outer}}}{\lambda}$ in all the three versions,

2. Version three (represented by the dash-cross, the dashed-circle and the dashed-diamond curves) has the lowest CRB (best estimation accuracy) for the number of sensors less than 16 but the highest CRB (poorest estimation accuracy) for the number of sensors greater than 16 at all values of $\frac{R_{\mathrm{outer}}}{\lambda}$,

3. Version one (represented by the solid, the dashed-dot and the dashed curves) has the highest CRB (poorest estimation accuracy) for the number of sensors less than 16 but the lowest CRB (best estimation accuracy) for the number of sensors greater than 16 at all values of $\frac{R_{\mathrm{outer}}}{\lambda}$, and

4. All the three versions have exactly equal estimation accuracy at 16 number of sensors since at this point, each ring in each of the three versions has equal (8) number of sensors.

5.2 Conclusion

This project proposed a new concentric circular sensor-array grid termed as the 2-circle concentric uniform array geometry. This proposed geometry increased the array's spatial aperture while maintaining the inter-sensor spacing not to exceed half a wavelength and offered all the advantages of a single-ring array geometry with minimal mutual coupling effects. The study derived both the array manifolds and the Cramér-Rao bounds for the proposed geometry and that of the single ring array geometry termed as uniform circular array (UCA). Via the Cramér-Rao bound analysis, a better-accurate performance in direction finding of the proposed array grid over that of the UCA was analytically verified. Further, the performance in direction finding of the proposed array grid and that of the uniform circular array was compared graphically under different constraints of investigation. It was found that, the Cramér-Rao bound decreases with increase in the number of sensors and/or the radii (increase in array's spatial aperture). The proposed array grid was found to have the lowest CRBs and thus had better estimation accuracy than the single ring array. Additionally, The 2-circle concentric uniform array would have the best estimation accuracy if minimal (≤ 16) number of sensors is adopted and hence reducing hardware cost.

5.3 Recommendation

On completion of the study, the following recommendations were made

1. The inter-sensor spacing should be less or equal to half a wavelength,
2. The 2-circle concentric uniform array geometry should be used for direction finding as opposed to the uniform circular array geometry
3. The minimal number of sensors should be used for direction finding to minimize hardware cost

REFERENCES

[1] S. M. Kay, *Fundamental of Statistical Signal Processing: Estimation Theory*, Upper Saddle River, New Jersey, USA: Prentice Hall, April 1993.

[2] K. T. Wong and M. D. Zoltowski, "Extended-aperture underwater acoustic multisource azimuth/elevation direction-finding using uniformly but sparsely spaced vector hydrophones," *IEEE Journal of Oceanic Engineering*, vol. 22, no. 4, pp. 659-672, October 1997.

[3] K. T. Wong and M. D. Zoltowski, "Self-initiating MUSIC-based direction finding and polarization estimation in spatio-polarizational beamspace," *IEEE Transactions on Antennas and Propagation*, vol. 48, no. 8, pp. 1235-1245, august 2000.

[4] M. D. Zoltowski and K. T. Wong, "ESPRIT-based 2-D direction finding with a sparse uniform array of electromagnetic vector sensors," *IEEE Transactions on Signal Processing*, vol. 48, no. 8, pp. 2195-2204, August 2000.

[5] H. L. Van Trees, *Detection, Estimation and Modulation Theory, Part IV: Optimum Array Processing*, New York, USA: John Wiley and Sons, 2002.

[6] S. A. Vorobyov, A. B. Gershman, and K. M. Wong "Maximum likelihood direction-of-arrival estimation in unknown noise fields using sparse sensor arrays," *IEEE Transactions on Signal Processing*, vol. 53, no. 1, pp. 34-43, January 2005.

[7] N. Tayem and H. M. Kwon, "L-shape 2-dimensional arrival angle estimation with propagator method," *IEEE Transactions on Antennas and Propagation*, vol. 53, no. 5, pp. 1622-1630, May 2005.

[8] T. G. Spence and H. W. Douglas, "Design of broadband planar arrays based on the optimization of aperiodic tilings," *IEEE Transactions on Antennas and Propagation*, vol. 56, no. 1, pp. 76-86, January 2008.

[9] R. L. Haupt, "Optimized element spacing for low sidelobe concentric ring arrays," *IEEE Transactions on Antennas and Propagation*, vol. 56, no. 1, pp. 266-268, January 2008.

[10] B. Friedlander, *Wireless Direction-Finding Fundamentals in Classical and Modern Direction-of-Arrival Estimation*, pp. 1-51, New york, USA, Elsevier Inc. 2009.

[11] M. Alvarez-Folgueiras, A R.-G.Juan, and A.-P. Francisco, "High-performance uniformly excited linear and planar arrays based on linear semiarrays composed of subarrays with different uniform spacings," *IEEE Transactions on Antennas and Propagation*, vol. 57, no. 12, pp. 4002-4006, December 2009.

[12] S. Rhode, "Introduction into theory of direction finding, radiomonitoring and radiolocation," *International Journal of Computer Applications* ,vol. 6, no. 3, pp.26-49, August 2010.

[13] M. J. Abedin and A. S. Mohan, "Maximum likelihood near field localisation using concentric circular ring array," *IEEE International Conference on Electromagnetics in Advanced Applications*, pp. 533-536, 2010.

[14] C. Hui and B. Zheng, "Performance analysis of self-calibration algorithm for concentric-UCA," *IEEE International Conference on Wireless Communications and Signal Processing*, 2010.

[15] F. Castanie, *Digital Spectral Analysis: Parametric, Non-Parametric and Advanced Methods*, New York, USA: Wiley and Sons, 2013.

[16] B. Liao and S. C. Chan, "Direction finding with partly calibrated uniform linear arrays," *IEEE Transactions on Antennas and Propagation*, vol. 60, no. 2, pp. 922-929, February 2012.

[17] U. Singh and T. S. Kamal, "Synthesis of thinned planar concentric circular antenna arrays using biogeography-based optimisation," *IET Microwaves, Antennas and Propagation*, vol. 6, no. 7, pp. 822-829, May 2012.

[18] L. Zhang, Y.-C. Jiao, B. Chen and Z.-B. Weng, "Design of wideband concentric-ring arrays with three-dimensional beam scanning based on the optimization of array geometry," *Electromagnetics*, vol. 32, no. 6, pp. 305-320, July 2012.

[19] S. Akkar, F. Harabi, and A. Gharsallah, "Concentric circular-shaped electronically steerable parasitic array radiator antennas for full-azimuth directions of arrival estimation with reduced computational load," *IET Microwaves, Antennas and Propagation*, vol. 6, no. 11, pp. 1236-1243, August 2012.

[20] M. D. Gregory, F. A. Namin, and D. H. Werner, "Exploiting rotational symmetry for the design of ultra-wideband planar phased array layouts," *IEEE Transactions on Antennas and Propagation*, vol. 61, no. 1, pp. 176-184, January 2013.

[21] V. Krishnaveni, T. Kesavamurthy, and B. Aparna. "Beamforming for direction-of-arrival (DOA) estimation-a survey," *International Journal of Computer Applications*, vol. 61, no. 11, January 2013.

[22] D. T. Vu, R. Alexandre, B. Rémy, and M. Sylvie, "A Cramér Rao bounds based analysis of 3D antenna array geometries made from ULA branches," *Multidimensional Systems and Signal Processing*, vol. 24, no. 1, pp. 121-155, March 2013.

[23] B. Liao, K.-M. Tsui, and S.-C. Chan, "Frequency invariant uniform concentric circular arrays with directional elements," *IEEE Transactions on Aerospace and Electronic Systems*, vol. 49, no. 2, pp. 871-884, April 2013.

[24] Y. Jiang and Z. Shu, "An innovative strategy for synthesis of uniformly weighted circular aperture antenna array based on the weighting density method," *IEEE Antennas and Wireless Propagation Letters*, vol. 12, pp. 725-728, 2013.

[25] P. H. Leong, T. D. Abhayapala, and T. A. Lamahewa, "Multiple target localization using wideband echo chirp signals," *IEEE Transactions on Signal Processing*, vol. 61, no. 16, pp. 4077-4089, August 2013.

[26] C. K. H. Sanvidha and P. N. Pathirana, "Optimal sensor arrangements in angle of arrival (AoA) and range based localization with linear sensor arrays," *IEEE Sensors Journal*, vol. 13, no. 9, pp. 12277-12294, September 2013.

[27] L. Wang, G. Wang, and Z. Chen, "Joint DOA-polarization estimation based on uniform concentric circular array," *Journal of Electromagnetic Waves and Applications*, vol. 27, no. 13, pp. 1702-1714, September 2013.

[28] J. P. Delmas, "Performance bounds and statistical Analysis of DOA estimation," *In Academic Press Library in Signal Processing*, vol. 3, pp. 719-764. Elsevier, 2014.

[29] G. Ram, D. Mandal, R. Kar, and S. P. Ghoshal, "Circular and concentric circular antenna array synthesis using cat swarm optimization," *IETE Technical Review*, vol. 32, no. 3, pp. 204-217, May 2015.

[30] B. N. Bansode and N. A. Dheringe, "Performance evaluation and analysis of direction of arrival estimation using MUSIC, TLS ESPRIT and Pro ESPRIT algorithms," *International Journal of Advanced Research in Electrical, Electronics and Instrumentation Engineering*, vol. 04, no. 06, pp. 4948-4958, June 2015.

[31] M. Devendra and K. Manjunathachari, "Solar DC microgrid for rural electrification: A case study," *International Advanced Research Journal in Science, Engineering and Technology (IARJSET)*, vol. 2, no. 1, pp. 1-5, 2015.

[32] K. Chen, H. Chen, L. Wang, and H. Wu, "Modified real ga for the synthesis of sparse planar circular arrays," *IEEE Antennas Wireless Propagation Letters*, vol. 15, pp. 274-277, June 2016.

[33] D. M. Kitavi, T.-C. Lin, and K. T. Wong, "A tetrahedral array of isotropic sensors, each suffering a random complex gain?the resulting hybrid Cramér-Rao bound for direction finding," *IEEE national conference On Aerospace and Electronics Conference (NAECON) and Ohio Innovation Summit (OIS)*, pp. 412-415, July 2016.

[34] H. Gazzah, J. Delmas, and S. M. Jesus, "Direction-finding arrays of directional sensors for randomly located sources," *IEEE Transactions on Aerospace and Electronic Systems*, vol. 52, no. 4, pp. 1995-2003, August 2016.

[35] D. M. Kitavi, T.-C. Lin, K. T. Wong, and Y. I. Wu, "Direction finding with the sensors' gains suffering Bayesian uncertainty - hybrid CRB and MAP estimation," *IEEE Transactions on Aerospace and Electronic Systems*, vol. 52, no. 4, pp. 2038-2044, August 2016.

[36] D. M. Kitavi, T. Hao, and K. T. Wong, "A regular tetrahedral array whose constituent sensors fail randomly?A lower bound for direction-of-arrival estimation," *IEEE conference on Antennas and Propagation*, pp. 1-5., November 2016.

[37] D. M. Kitavi, K. T. Wong, and C.-C. Hung, "An L-shaped array with nonorthogonal axes' its Cramér-Rao bound for direction finding," *IEEE Transactions on Aerospace and Electronic Systems*, vol. 54, no. 1, pp. 486-492, February 2017.

[38] D. M. Kitavi, K. T. Wong, M. Zou, and K. Agrawal, "A lower bound of the estimation error of an emitter's direction of arrival/polarization for collocated triad of orthogonal dipoles/loops that fail randomly," *IET Microwaves, Antennas, and Propagation*, vol. 11, no. 7, pp. 961-970, June 2017.

[39] X. Zhao, Y. Zhang, and Q. Yang, "Synthesis of sparse concentric ring arrays based on Bessel function," *IET Microwaves, Antennas and Propagation* vol. 11, no. 11, pp. 1651-1660, June 2017.

[40] D. Kajaree and R. Behera, "A survey on web crawler approaches," *International Journal of Innovative Research in Computer and Communication Engineering*, vol. 5, no. 2, pp. 1302-1309, 2017.

[41] K. T. Wong, S. Yang, J. F. Caleb, K. Salman, and T. Wai-Yip, "Electrically ?Long? Dipoles in a Collocated/Orthogonal Triad?for Direction Finding and Polarization Estimation," *IEEE Transactions on Antennas and Propagation*, vol. 65, no. 11, pp. 6057-6067, November 2017.

[42] K. T. Wong, J. N. Chibuzo, and I. W. Yue, "A triad of cardioid sensors in orthogonal orientation and spatial collocation?Its spatial-matched-filter-type beam-pattern," *IEEE Transactions on Signal Processing*, vol. 66, no. 4, pp. 895-906, February 2018.

[43] S. Khan, K. T. Wong, S. Yang, and T. Wai-Yip, "Electrically Large Circular Loops in the Estimation of an Incident Emitter?s Direction-of-Arrival or Polarization," *IEEE Transactions on Antennas and Propagation*, vol. 66, no. 6, pp. 3046-3055, June 2018.

[44] J. O. Kim, D. J. Hwang, H. W. Paek, and C. H. Chung, "An application of the merging algorithm with the discrete wavelet transform to extract valid speech-sound," *IEEE International Workshop on Virtual and Intelligent Measurement Systems*, pp. 67-70, 2001.

[45] A. Dogandzic and A. Nehorai, "Cramer-Rao bounds for estimating range, velocity, and direction with an active array," *IEEE transactions on Signal Processing*, vol. 49, no. 6, pp.1122-1137, June 2001.

[46] H. Scott and V. F. Fusco, "360/spl deg/electronically controlled beam scan array," *IEEE Transactions on Antennas and Propagation*, vol. 52, no. 1, pp. 333-335, January 2004.

[47] H. Abeida and D. Jean-Pierre, "Gaussian Cramer-Rao bound for direction estimation of non-circular signals in unknown noise fields," *IEEE Transactions on Signal Processing*, vol. 53, no. 12, pp. 4610-4618, May 2005.

[48] P. Ioannides and B. A. Constantine, "Uniform circular arrays for smart antennas," *IEEE Antennas and Propagation Magazine*, vol. 47, no. 4, pp. 192-206, August 2005 .

[49] Y. Sasaki, Y. Tamai, S. Kagami, and H. Mizoguchi, "2D sound source localization on a mobile robot with a concentric microphone array," *IEEE International Conference on Systems, Man and Cybernetics*, vol. 4, pp. 3528-3533, 2005.

[50] Y. Wu and S. C. Hing, "Simple and accurate two-dimensional angle estimation for a single source with uniform circular array," *IEEE Antennas and Wireless Propagation Letters*, vol. 7, pp. 78-80, April 2008.

[51] G. Efstathopoulos and A. Manikas, "Extended array manifolds: Functions of array manifolds," *IEEE Transactions on Signal Processing*, vol. 59, no. 7, pp. 3272-3287, July 2011.

[52] S. Abdus, Encyclopedia of Research Design: *Unbiased Estimator*. Thousand Oaks, USA. SAGE Publications, Inc, 2012.

[53] R. Eirey-Perez, J. A. Rodriguez-Gonzalez, and F. J. Ares-Pena, "Realizing - symmetric radiation patterns of circular apertures using circular square-grid arrays [antenna designer's notebook]," *IEEE Antennas and Propagation Magazine*, vol. 54, no. 3, pp. 135-142, June 2012.

[54] D. Bianchi, G. Simone, and M. Agostino, "Constrained Pareto optimization of wide band and steerable concentric ring arrays," *IEEE Transactions on Antennas and Propagation*, vol. 60, no. 7, pp. 3195-3204, July 2012.

[55] R. Kutil, "Biased and unbiased estimation of the circular mean resultant length and its variance," *Statistics*, vol. 46, no. 4, pp. 549-561, August 2012.

[56] H. Gazzah and D. Jean-Pierre, "Direction finding antenna arrays for the randomly located source," *IEEE Transactions on Signal Processing*, vol. 60, no. 11, pp. 6063-6068, November 2012.

[57] M. Li, L. Yilong, and B. He, "Array signal processing for maximum likelihood direction-of-arrival estimation," *Journal of Electrical and Electronic Systems*, vol. 3, no. 1, pp. 117, December 2013.

[58] X. Lan, L. Wan, G. Han, and J. Rodrigues, "A novel DOA estimation algorithm using array rotation technique," *Future Internet*, vol. 6, no. 1, pp. 155-170, March 2014.

[59] P. Angeletti, T. Giovanni, and R. Gianfranco, "Array antennas with jointly optimized elements positions and dimensions part II: Planar circular arrays," *IEEE Transactions on Antennas and Propagation*, vol. 62, no. 4, pp. 1627-1639, April 2014.

[60] R. A. Mendez, J. F. Silva, R. Orsotica, and R. Lobos, "Analysis of the Cramer-Rao lower uncertainty bound in the joint estimation of astrometry and photometry," *Publications of the Astronomical Society of the Pacific*, vol. 126, no. 942, pp. 798-810, 2014.

[61] J. Brad, B. Liao, S. Rajan, and S. Wang, "Theory, design, and measurement of novel uniform circular antenna arrays for direction of arrival estimation," *Defence Research and Development Canada-Ottawa Research Centre Ottawa ON Canada*, pp. 80 January 2015.

[62] G. Ram, D. Mandal, R. Kar, and S. P. Ghoshal, "Cat swarm optimization as applied to time-modulated concentric circular antenna array: Analysis and comparison with other stochastic optimization methods," *IEEE Transactions on Antennas and Propagation*, vol. 63, no. 9, pp. 4180-4183, September 2015.

[63] M. Devendra and K. Manjunathachari, "Solar DC microgrid for rural electrification: A case study," *International Advanced Research Journal in Science, Engineering and Technology (IARJSET)*, vol. 2, no. 1, pp. 1-5, 2015.

[64] D. M. Kitavi, T. C. Lin, and K. T. Wong, "A tetrahedral array of isotropic sensors, each suffering a random complex gain -The resulting hybrid CramÃ©r-Rao bound for direction finding," *Proceedings of the IEEE National Aerospace Electronics Conference*, NAECON, pp. 412-415, July 2016.

[65] J. Steinwandt, R. Florian, H. Martin, and D. G. Giovanni, "Deterministic Cramer-Rao bound for strictly non-circular sources and analytical analysis of the achievable gains," *IEEE Transactions on Signal Processing*, vol. 64, no. 17, pp. 4417-4431, September 2016.

[66] D. M. Kitavi, k. T. wong, and C. Hung, "An L-shaped array with nonorthogonal axes-its 2 Cramer-Rao bound for direction finding," *IEEE Transactions on Aerospace and Electronic Systems*, vol. 54, no. 1, pp. 486-492, February 2017.

[67] W. Jiang and H. M. Alexander, "Cramer-Rao bound for noncoherent direction of arrival estimation in the presence of sensor location errors," *IEEE Signal Processing Letters*, vol. 24, no. 9, pp. 1303-1307, September 2017.

[68] O. Elizarraras, A. Marco, M. A. Panduro, Alberto Reyna, and C. H. David, "Design of circular antenna arrays of circular subarrays exploiting rotational symmetry," *Journal of Electromagnetic Waves and Applications*, vol. 31, no. 13, pp. 1277-1288, September 2017.

[69] A. Ghani, K. Firooz, and S. H. Seyed, "Antenna array placement on limited bound for isotropic and optimal direction-of-arrival estimation," *IET Signal Processing*, vol. 12, no. 3, pp. 277-283, October 2017.

[70] G. M. Pralon, G. D.Giovanni, L. Markus, H. A. Matthias, and T. S. Reiner, "Suitability of compact antenna arrays for direction-of-arrival estimation," *IEEE Transactions on Antennas and Propagation*, vol. 65, no. 12, pp. 7244-7256, December 2017.

[71] C. O. Stearns and A. C. Stewart, "An investigation of concentric ring antennas with low sidelobes," *IEEE Transactions on Antennas and Propagation*, vol. 13, no. 6, pp. 856-863, November 1965.

[72] R. Das, "Concentric ring array," *IEEE Transactions on Antennas and Propagation*, vol. 14, no. 3, pp. 398-400, May 1966.

[73] A. K. Bhattacharyya and R. Garg, "A microstrip array of concentric annular rings," *IEEE Transactions on Antennas and Propagation*, vol. 33, no. 6, pp. 655-659, June 1985.

[74] L. Kumar and H. M. Rajesh, "Stochastic Cramer-Rao bound analysis for DOA estimation in spherical harmonics domain," *IEEE Signal Processing Letters*, vol. 22, no. 8, pp. 1030-1034, August 2015.

[75] S. Peng, C.-W. Yuan, T. Shu, J. Ju, and Q. Zhang, "Design of a concentric array radial line slot antenna for high-power microwave application," *IEEE Transaction on Plasma Science*, vol. 43, no. 10, pp. 3527-3529, October 2015.

[76] X. Zhao, Q. Yang, and Y. Zhang, "A hybrid method for the optimal synthesis of 3-D patterns of sparse concentric ring arrays," *IEEE Transactions on Antennas and Propagation*, vol. 64, no. 2, pp. 515-524, February 2016.

[77] D. M. Kitavi, T.-C. Lin, K. T. Wong, and Y. I. Wu, "Direction finding with the sensors' gains suffering Bayesian uncertainty - hybrid CRB and MAP estimation," *IEEE Transactions on Aerospace and Electronic Systems*, vol. 52, no. 4, pp. 2038-2044, August 2016.

[78] J. Steinwandt, R. Florian, H. Martin, and D. G. Giovanni, "Deterministic Cramer-Rao bound for strictly non-circular sources and analytical analysis of the achievable gains," *IEEE Transactions on Signal Processing*, vol. 64, no. 17, pp. 4417-4431, September 2016.

Appendix 1: Expansion of Series in (4.27) − (4.31)

The series in (4.27):

$$\begin{aligned}
&\sum_{\ell=1}^{L} \cos^2\left(\phi - \frac{2\pi(\ell-1)}{L}\right) \\
=\ &\sum_{\ell=0}^{L-1} \cos^2\left(\frac{2\pi\ell}{L} - \phi\right) \\
=\ &\sum_{\ell=0}^{L-1} \left[\cos(\phi)\cos\left(\frac{2\pi\ell}{L}\right) + \sin(\phi)\sin\left(\frac{2\pi\ell}{L}\right)\right]^2 \\
=\ &\cos^2(\phi)\sum_{\ell=0}^{L-1} \cos^2\left(\frac{2\pi\ell}{L}\right) + \sin^2(\phi)\sum_{\ell=0}^{L-1} \sin^2\left(\frac{2\pi\ell}{L}\right) + \frac{\sin(2\phi)}{2}\sum_{\ell=0}^{L-1} \sin\left(\frac{4\pi\ell}{L}\right) \qquad (17)
\end{aligned}$$

The series in (4.29):

$$\begin{aligned}
&\sum_{\ell=1}^{L} \sin^2\left(\phi - \frac{2\pi(\ell-1)}{L}\right) \\
=\ &\sum_{\ell=0}^{L-1} \sin^2\left(\frac{2\pi\ell}{L} - \phi\right) \\
=\ &\sum_{\ell=0}^{L-1} \left[\cos(\phi)\sin\left(\frac{2\pi\ell}{L}\right) - \sin(\phi)\cos\left(\frac{2\pi\ell}{L}\right)\right]^2 \\
=\ &\cos^2(\phi)\sum_{\ell=0}^{L-1} \sin^2\left(\frac{2\pi\ell}{L}\right) + \sin^2(\phi)\sum_{\ell=0}^{L-1} \cos^2\left(\frac{2\pi\ell}{L}\right) - \frac{\sin(2\phi)}{2}\sum_{\ell=0}^{L-1} \sin\left(\frac{4\pi\ell}{L}\right) \qquad (18)
\end{aligned}$$

The series in (4.31):

$$\begin{aligned}
&\sum_{\ell=1}^{L} \sin\left(2\phi - \frac{4\pi(\ell-1)}{L}\right) \\
=\ &\sum_{\ell=0}^{L-1} \sin\left(\frac{4\pi\ell}{L} - 2\phi\right) \\
=\ &\sum_{\ell=0}^{L-1} \cos(2\phi)\sin\left(\frac{4\pi\ell}{L}\right) - \sin(2\phi)\sum_{\ell=0}^{L-1} \cos\left(\frac{4\pi\ell}{L}\right) \qquad (19)
\end{aligned}$$

(17) − (19) depend on the series $\sum_{\ell=0}^{L-1}\cos^2\left(\frac{2\pi\ell}{L}\right)$, $\sum_{\ell=0}^{L-1}\sin^2\left(\frac{2\pi\ell}{L}\right)$, $\sum_{\ell=0}^{L-1}\cos\left(\frac{4\pi\ell}{L}\right)$, and $\sum_{\ell=0}^{L-1}\sin\left(\frac{4\pi\ell}{L}\right)$, which are solved as follows:

$$\begin{aligned}
&\sum_{\ell=0}^{L-1}\cos^2\left(\frac{2\pi\ell}{L}\right)\\
&= 1+\cos^2\left(\frac{2\pi}{L}\right)+\cos^2\left(\frac{4\pi}{L}\right)+\cdots+\cos^2\left(\frac{2\pi(L-1)}{L}\right)\\
&= 1+\cos^2(\gamma)+\cos^2(2\gamma)+\cdots+\cos^2((L-1)\gamma)\\
&= 1+\frac{1+\cos(2\gamma)}{2}+\cdots+\frac{1+\cos(2(L-1)\gamma)}{2}\\
&= \frac{1}{2}\left[2+1+\cos(2\gamma)+1+\cos(4\gamma)+\cdots+1+\cos(2(L-1)\gamma)\right]\\
&= \frac{1}{2}\left[L+1+\cos(2\gamma)+\cos(4\gamma)+\cdots+\cos(2(L-1)\gamma)\right]\\
&= \frac{1}{2}\left[L+1+\cos(\delta)+\cos(2\delta)+\cdots+\cos((L-1)\delta)\right] \qquad (20)
\end{aligned}$$

Now, using a known series

$$\begin{aligned}
&\cos(\beta)+\cos(2\beta)+\cos(3\beta)+\cos(4\beta)+\cdots\cos((n-1)\beta)+\cos(n\beta)\\
=\ &\frac{\sin\left((n+\frac{1}{2})\beta\right)-\sin\left(\frac{1}{2}\beta\right)}{2\sin\left(\frac{1}{2}\beta\right)}
\end{aligned}$$

, we have

$$\begin{aligned}
\sum_{\ell=0}^{L-1}\cos^2\left(\frac{2\pi\ell}{L}\right) &= \frac{1}{2}\left[L+1+\frac{\sin\left((L+\frac{1}{2})\delta\right)-\sin\left(\frac{1}{2}\delta\right)}{2\sin\left(\frac{1}{2}\delta\right)}-\cos(L\delta)\right]\\
&= \frac{1}{2}\left[L+1+\frac{\sin\left(4\pi+\frac{2\pi}{L}\right)-\sin\left(\frac{2\pi}{L}\right)}{2\sin\left(\frac{2}{L}\pi\right)}-\cos(4\pi)\right]\\
&= \frac{1}{2}\left[L+\frac{\sin\left(4\pi+\frac{2\pi}{L}\right)-\sin\left(\frac{2\pi}{L}\right)}{2\sin\left(\frac{2\pi}{L}\right)}\right]\\
&= \frac{L}{2} \qquad (21)
\end{aligned}$$

(21) is obtained by the use of trigonometric identity, $\sin(A+B) = \sin(A)\cos(B) + \cos(A)\sin(B)$ which implies that $\sin(4\pi+\frac{2\pi}{L}) = \sin(4\pi)\cos\left(\frac{2\pi}{L}\right)+\cos(4\pi)\sin\left(\frac{2\pi}{L}\right) = \sin\left(\frac{2\pi}{L}\right)$

For $\sum_{\ell=0}^{L-1} \sin^2\left(\frac{2\pi\ell}{L}\right)$ using the trigonometric identity $\sin^2(\alpha) = \frac{1-\cos(2\alpha)}{2}$ we have,

$$\begin{aligned}
&\sum_{\ell=0}^{L-1} \sin^2\left(\frac{2\pi\ell}{L}\right) \\
&= \sin^2\left(\frac{2\pi}{L}\right) + \sin^2\left(\frac{4\pi}{L}\right) + \cdots + \sin^2\left(\frac{2\pi(L-1)}{L}\right) \\
&= \sin^2(\gamma) + \sin^2(2\gamma) + \cdots + \sin^2((L-1)\gamma) \\
&= \frac{1-\cos(2\gamma)}{2} + \cdots + \frac{1-\cos(2(L-1)\gamma)}{2} \\
&= \frac{1}{2}\left[1-\cos(2\gamma)+1-\cos(4\gamma)+\cdots+1-\cos(2(L-1)\gamma)\right] \\
&= \frac{1}{2}\left[(L-1)-(\cos(2\gamma)+\cos(4\gamma)+\cdots+\cos(2(L-1)\gamma))\right]. \qquad (22)
\end{aligned}$$

Using the same procedure for (21) in (24), it is clear that,

$$\begin{aligned}
1+\cos(2\gamma)+\cos(4\gamma)+\cdots+\cos(2(L-1)\gamma) &:= \sum_{\ell=0}^{L-1}\cos\left(\frac{2\pi\ell}{L}\right) \\
&= 0. \qquad (23)
\end{aligned}$$

Thus,

$$\begin{aligned}
\sum_{\ell=0}^{L-1} \sin^2\left(\frac{2\pi\ell}{L}\right) &= \frac{1}{2}\left[L-(1+\cos(2\gamma)+\cos(4\gamma)+\cdots+\cos(2(L-1)\gamma))\right] \\
&= \frac{L}{2}. \qquad (24)
\end{aligned}$$

Finally,

$$\begin{aligned}
\sum_{\ell=0}^{L-1} \sin\left(\frac{2\pi\ell}{L}\right) &= \sin\left(\frac{2\pi}{L}\right) + \sin\left(\frac{4\pi}{L}\right) + \cdots + \sin\left(\frac{2\pi(L-1)}{L}\right) \\
&= \sin(\gamma) + \sin(2\gamma) + \cdots + \sin((L-1)\gamma)
\end{aligned}$$

Here, we further make use of the following trigonometric series expansion:

$$\begin{aligned}
&\sin(\beta) + \sin(2\beta) + \sin(3\beta) + \sin(4\beta) + \cdots \sin((n-1)\beta) + \sin(n\beta) \\
= \; &\frac{\cos\left(\frac{1}{2}\beta\right) - \cos\left((n+\frac{1}{2})\beta\right)}{2\sin\left(\frac{1}{2}\beta\right)}.
\end{aligned}$$

Therefore,

$$\begin{aligned}\sum_{\ell=0}^{L-1}\sin\left(\frac{2\pi\ell}{L}\right) &= \frac{\cos\left(\frac{1}{2}\gamma\right)-\cos\left((L+\frac{1}{2})\gamma\right)}{2\sin\left(\frac{1}{2}\gamma\right)}-\sin\left(L\gamma\right)\\ &= \frac{\cos\left(\frac{2\pi}{L}\right)-\cos\left(4\pi+\frac{2\pi}{L}\right)}{2\sin\left(\frac{1}{2}\gamma\right)}-\sin\left(4\pi\right)\\ &= 0 \qquad (25)\end{aligned}$$

since $\cos(A+B)=\cos(A)\cos(B)-\sin(A)\sin(B)$ which implies that $\cos(4\pi+\frac{2\pi}{L})=\cos(4\pi)\cos\left(\frac{2\pi}{L}\right)-\sin(4\pi)\sin\left(\frac{2\pi}{L}\right)=\cos\left(\frac{2\pi}{L}\right)$. Therefore, using (21) – (25) in (17) – (19) the results in (4.27) – (4.31) are obtained.

Appendix 2: Publications

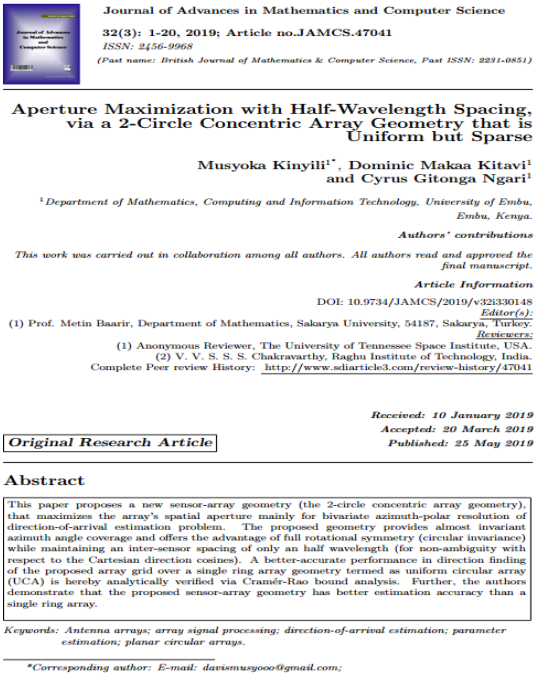

Journal of Advances in Mathematics and Computer Science

32(3): 1-20, 2019; Article no.JAMCS.47041
ISSN: 2456-9968
(Past name: British Journal of Mathematics & Computer Science, Past ISSN: 2231-0851)

Aperture Maximization with Half-Wavelength Spacing, via a 2-Circle Concentric Array Geometry that is Uniform but Sparse

Musyoka Kinyili[1*], Dominic Makaa Kitavi[1] and Cyrus Gitonga Ngari[1]

[1]Department of Mathematics, Computing and Information Technology, University of Embu, Embu, Kenya.

Authors' contributions

This work was carried out in collaboration among all authors. All authors read and approved the final manuscript.

Article Information

DOI: 10.9734/JAMCS/2019/v32i330148
Editor(s):
(1) Prof. Metin Baarir, Department of Mathematics, Sakarya University, 54187, Sakarya, Turkey.
Reviewers:
(1) Anonymous Reviewer, The University of Tennessee Space Institute, USA.
(2) V. V. S. S. S. Chakravarthy, Raghu Institute of Technology, India.
Complete Peer review History: http://www.sdiarticle3.com/review-history/47041

Received: 10 January 2019
Accepted: 20 March 2019
Published: 25 May 2019

Original Research Article

Abstract

This paper proposes a new sensor-array geometry (the 2-circle concentric array geometry), that maximizes the array's spatial aperture mainly for bivariate azimuth-polar resolution of direction-of-arrival estimation problem. The proposed geometry provides almost invariant azimuth angle coverage and offers the advantage of full rotational symmetry (circular invariance) while maintaining an inter-sensor spacing of only an half wavelength (for non-ambiguity with respect to the Cartesian direction cosines). A better-accurate performance in direction finding of the proposed array grid over a single ring array geometry termed as uniform circular array (UCA) is hereby analytically verified via Cramér-Rao bound analysis. Further, the authors demonstrate that the proposed sensor-array geometry has better estimation accuracy than a single ring array.

Keywords: Antenna arrays; array signal processing; direction-of-arrival estimation; parameter estimation; planar circular arrays.

**Corresponding author: E-mail: davismusyooo@gmail.com;*

Figure 13: Publication one

Academic Paper Acceptance Letter
DOI of the journal: 10.7176/MTM

Dear Musyoka KINYILI, Dominic Makaa KITAVI, and Cyrus Gitonga NGARI,

It's my pleasure to inform you that, after the peer review, your paper,

Sensors' Distribution Based Estimation Accuracy of 3-Versions 2-Ring Concentric Uniform Planar Arrays

has been ACCEPTED with content unaltered to publish with **Journal of Mathematical Theory and Modeling**, ISSN (Paper)2224-5804 ISSN (Online)2225-0522.

In order to fit into the publishing and printing schedule, please re-submit your complete publication package by directly replying this acceptance email within 15 days so we can make your article available online/print in the next issue (usually at the end of each month) . If you failed to prepare your complete files on time, the publication of your article might be delayed.

Though the reviewers of the journal already confirmed the quality of your paper's current version, you can still add content to it, such as solidifying the literature review, adding more content in the conclusion, giving more information on your analytical process and giving acknowledgement.

To help the editor of the journal process your final paper quickly, you need to prepare your paper based on the attached "publication_package_instruction.pdf".

Again, thank you for working with IISTE. I believe that our collaboration will help to accelerate the global knowledge creation and sharing one step further. IISTE looks forward to your final publication package. Please do not hesitate to contact me if you have any further questions.

Sincerely,

Alexander Decker,
Tuesday, June 04, 2019

Editor-in-Chief
IISTE-Accelerating Global Knowledge Sharing
The International Institute for Science, Technology and Education

The indexation of the journal

IISTE would like to acknowledge the supports from co-hosting universities worldwide

- University of North Carolina at Charlotte, United States
- California State University, United States
- The City University of New York, United States

INTERNATIONAL INSTITUTE FOR SCIENCE, TECHNOLOGY AND EDUCATION (IISTE) is a voting member of CrossRef
http://www.crossref.org/01company/17crossref_members.html

Figure 14: Publication two